Intermolecular interactions of the extended recognition site of VIM -2 metallo-β-lactamase with 1,2,4-triazole-3-thione inhibitors. Validations of a polarizable molecular mechanics potential by ab initio QC

Karolina Kwapien, Laurent Gavara, Jean-denis Docquier, Dorothée Berthomieu, Jean-François Hernandez, Nohad Gresh

Journal of COMPUTATIONAL CHEMISTRY

Intermolecular interactions of the extended recognition site of VIM-2 MBL with 1,2,4-triazole-3-thione inhibitors. Validations of a polarizable molecular mechanics/dynamics potential by ab initio QC:

Journal:	*Journal of Computational Chemistry*
Manuscript ID	JCC-20-0390
Wiley - Manuscript type:	Full Paper
Date Submitted by the Author:	30-Jul-2020
Complete List of Authors:	Kwapien, Karolina; Sygnature Discovery Ltd Gavara, Laurent; Institut des Biomolécules Max Mousseron, UMR5247 CNRS, Université de Montpellier,Faculté de Pharmacie, 34093 Montpellier Cedex 5, France Docquier, Jean-Denis; eDipartimento di Biotecnologie Mediche, Università di Siena, I-53100 Siena, Italy. Berthomieu, Dorothee; Institut Charles Gerhardt de Montpellier Hernandez, Jean-Francois; Institut des Biomolécules Max Mousseron, UMR5247 CNRS, Université de Montpellier, ENSCM, Faculté de Pharmacie, 34093 Montpellier Cedex 5, France Gresh, Nohad; Laboratoire de Chimie Theorique, ;
Key Words:	Zn-metallo-□-lactamases; 1,2,4-triazole-3-thione inhibitors; polarizable molecular mechanics/dynamics; quantum chemistry, intermolecular interactions

Intermolecular interactions of the extended recognition site of VIM-2 Metallo-β-Lactamase with 1,2,4-triazole-3-thione inhibitors. Validations of a polarizable molecular mechanics/dynamics potential by ab initio QC.

Karolina Kwapien,[a-c,f] Laurent Gavara,[d] Jean-Denis Docquier,[e] Dorothée Berthomieu,[c] Jean-François Hernandez,[d] Nohad Gresh [b]

[a]Laboratoire de Chimie et Biochimie Pharmacologiques et Toxicologiques, Université de Paris, UMR8601, Paris, F-75006 France

[b]Laboratoire de Chimie Théorique, UMR7616, Sorbonne Université, CNRS, 75252, Paris, France

[c]Institut Charles Gerhardt, UMR5253, CNRS, Université de Montpellier, ENSCM, 34296 Montpellier Cedex 5, France

[d]Institut des Biomolécules Max Mousseron, UMR5247 CNRS, Université de Montpellier, ENSCM, Faculté de Pharmacie, 34093 Montpellier Cedex 5, France.

[e]Dipartimento di Biotecnologie Mediche, Università di Siena, I-53100 Siena, Italy.

[f]Present address: Sygnature Discovery, Nottingham, United Kingdom

Molecular dynamics on the complexes of inhibitors with Zn-metalloproteins are a privileged area of applications of polarizable molecular mechanics potentials. With which accuracy could these reproduce the QC intermolecular interaction energies in the mono- and the dizinc binding sites? If convincing, this could pave the way for PMM to emulate QM/MM procedures for full-fledged MD simulations on the entirety of the protein complexes. We considered the complexes of the extended recognition site of a Zn-dependent metallo-β-lactamase, VIM-2, responsible for nosocomial disease, with five newly synthesized inhibitors sharing an original dizinc binding group, 1,2,4-triazole-3-thione (TZT). We considered the energy-minimized structures of each of the five VIM-2 complexes obtained with the SIBFA potential. Energy decomposition analyses (EDA) at the HF level enabled to compare the QC and the SIBFA ΔE values and their contributions in the two mono-zinc cores and the dizinc core, with and without TZT, totaling thirty complexes. With one exception, the ΔE(QC) values were reproduced with relative errors <1.5%. We next considered the complex of the whole inhibitor with substituents in the *ortho* position and in the hydrazine site, with an extended model of VIM-2 recognition site, totaling up to 280 atoms. ΔE(SIBFA) could closely reproduce ΔE(QC). EDA analyses were resumed on the complexes of each inhibitor arm with its interacting VIM-2 residues. As a last step, EDA results at the correlated level with the B3LYP-D3 and ω-B97X-D functionals were analyzed for the mono- and dizinc sites enabling comparisons with dispersion-augmented ΔE(SIBFA) and correlated multipoles and polarizabilities.

Key words: metallo-β-lactamases; 1,2,4-triazole-3-thione inhibitors; polarizable molecular mechanics/dynamics; ab initio quantum chemistry; intermolecular interactions.

Introduction.

Zn(II)-metalloenzymes [1-3] should constitute a privileged domain of application for accurate, quantum-chemistry (QC) grounded polarizable molecular mechanics/dynamics (PMM/PMD) potentials [4-10]. The need for such potentials is made clear by the non-anisotropy and non-additivity of ΔE(QC) and its individual contributions, unraveled by numerous energy-decomposition analyses (EDA) of mono- and polyligated Zn(II) complexes [11-15].

Classical, non-polarizable point-charge force-fields cannot account for such effects. For such complexes, the most reliable approach is multilevel QM/MM [16-18] or QM coupled with Effective Fragment Potentials or Fragment-Based approaches [19-21]. In spite of very noteworthy recent computational speedup of the QM part [22], the CPU time remains dominated by it. In addition, the long-range effects extend far beyond the QM core, so that a polarizable MM periphery is desirable.

Semi-empirical DFT-Tight -Binding approaches are a worthy alternative [23, 24] but unless coupled to Molecular Mechanics to handle the periphery of the zinc cores have not been extended so far to long-duration Molecular Dynamics (MD).

On account of such limitations, it would be rewarding if polarizable potentials could act as a surrogate for QC in the actual QM core, and not only at its periphery. Some of the above-mentioned papers have evaluated how well the Sum of Interactions Between Fragments Ab initio computed (SIBFA) procedure could reproduce non-anisotropy and non-additivity of ΔE(QC) in a diversity of mono- and polyligated Zn(II) complexes [11-13, 15]. These validations were extended to Zn-metalloprotein complexes, for which the numerical values of ΔE(QC) and their trends in series of related inhibitors could be closely accounted for [25-27].

But is it possible to further fine-tune this potential, revisiting first the zinc core(s) and subsequently the periphery where the arms of diverse inhibitors bind and confer enhanced affinity and selectivity for a targeted metalloprotein?

Metallo-β-lactamases (MBL), which emerged three decades ago, are a class of Zn-metalloenzymes responsible for acquired resistance to many β-lactam antibiotics in bacterial opportunistic pathogens [Reviewed in 28-31] and against which there are presently no clinically useful inhibitors yet, whence a major health concern worldwide [32].

Among these, VIM subtypes (Verona-Integron Metallo-beta-lactamase), which are among the most widespread metallo-carbapenemases in Europe and North America, are able to hydrolyze almost all marketed β-lactams [32]. VIM-2 is an MBL enzyme produced by Gram-negative opportunistic pathogens exhibiting multi-drug resistance phenotypes and which are responsible for nosocomial infections. The present paper is a continuation of a previous work [33] which focused on the mono- and dizinc cores of the L1 and VIM-2 MBL enzymes and their interaction energies with an original Zn-binding motif, the 1,2,4-triazole-3-thione (TZT) heterocycle. TZT has a monoanionic pentacyclic ring with an extracyclic sulfur atom. The Zn(II) cation of the His3-binding site is bound by

one ring nitrogen (N^2), on which the anionic charge is partly delocalized, and the Zn(II) cation of the Cys-Asp-His binding site is bound by the extracyclic S atom. As a step forward, we now consider the interaction energies of five novel MBL inhibitors, synthesized and tested in our Laboratories [34]. They all have the same TZT acting as an anchor in the dizinc core, and two arms substituting the ring C^5 and the hydrazone end. These substituents are denoted as R1 and R2 (Figure 1).

Three inhibitors, MV4690, 4390 and 5064, have an R2 *o*-benzoic substituent. Compound JMV5069 has a m-biphenyl arm possessing a carboxylate at the *meta* position of the second phenyl ring. Compound JMV4684 displays a 2,4-dihydroxy-phenyl as R2 substituent.
As R1 substituent, compound 4690 has a 2-hydroxy-5-methoxy-phenyl, while compound 4390 possesses an unsubstituted benzene ring. Both compounds 4684 and 5069 have a 2,5-dihydroxy-phenyl moiety. Compound 5064 contains a 3,5-dichlorophenyl substituent (Figure 1).

The synthesis of a large number of TZT-based inhibitors was very recently reported, along with their inhibitory potencies on several clinically relevant MBLs. Along with VIM-2 and VIM-4, these included NDM-1 (New-Delhi Metallo-β-lactamase), and IMP-1 (Imipenemase). The free energies of binding of nine of these for VIM-2 were in addition measured by Isothermal Calorimetry, enabling to derive the separate contributions of enthalpy and entropy to ΔG [34].

A major objective is SIBFA MD simulations on the complexes of a diversity of TZT grounded inhibitors, completed with free energy perturbation (FEP) studies [35, 36]. It should be attained by the integration of this potential and its gradients, now effective in a massively parallel computer code, Tinker-HP [37]. Following SAPT/DFT-based analyses of $\Delta E(QC)$, it recently enabled the first SIBFA MD simulations on liquid water and comparison with experimental observables [Naseem-Khan et al., to be submitted]. Extensions to a diversity of biologically-relevant fragments are underway [El Ahdab et al., work in progress].

Considering the non-isotropy and non-additivity issues, and in view of safe FEP computations, it is essential to ensure beforehand that $\Delta E(SIBFA)$ can reproduce as closely as possible $\Delta E(QC)$ and its individual contributions in a diversity of complexes making up extended recognition sites of Zn-metalloproteins. These concern on the one hand the interactions of the TZT anchor with the mono- and dizinc cores, and on the other hand those of each arm with its interacting VIM-2 partners around the binuclear core.

The present comparisons will be done on the SIBFA energy-minimized complexes of VIM-2 with each inhibitor. In a first step, an extended recognition site is extracted encompassing the inhibitor and the VIM-2 relevant residues, together with the closest fourteen 'discrete' water molecules. For each inhibitor, five single-point SIBFA and QC calculations are then performed on this site. They bear on: the uncomplexed site a) without and b) with the discrete waters; c) the site complexed with the sole TZT anchor and without the waters; and the site complexed with the complete inhibitor d) without and e) with the structural waters.
Proceeding in this step-wise fashion could be highly instructive to trace possible shortcomings in the last stage, e), to one of the preceding stages.

Due to its 'proof of concept' nature, the present study will mostly focus on comparisons with QC HF ΔE calculations. Preliminary results from correlated calculations will be evaluated only at the end of this study. This choice is motivated by the following:
-Energy Decomposition Analyses (EDA) on multimolecular complexes delivering separate values of the first-order Coulomb (E_C) and exchange-repulsion (E_X) and second-order polarization (E_{pol}) and charge-transfer (E_{ct}) can presently only be done with EDAs at the HF level, specifically with the Reduced Variational Space (RVS) method [38]. The released ALMOEDA procedure [39], used in the last part of this work, does enable EDA for multimolecular complexes and at several possible correlation levels. However, it does not provide a separation of E_C and E_X within the first-order of ΔE, E_1. Were shortcomings of E_1(SIBFA) to be found in some of these complexes, it would not enable to trace back whether they originate from E_C, E_X, or possibly both;
-the automated Least-Squares Fit (LSQF) procedure integrated in the SIBFA code should enable to fit equally well the separate ΔE(HF) contributions and those from correlated ΔE, such as from Symmetry Adapted Perturbation Theory (SAPT [40, 41] provided correlated multipoles and polarizabilities are used. Previous papers on ligand-alkali cation complexes [42, 43], on stacked and H-bonded cytosine and guanine dimers [44] and on cation channeling along the z axis of stacked guanine tetramers [45] did show these to enable virtually equally as good reproductions of correlated ΔE as of HF ΔE with uncorrelated multipoles and polarizabilities;
-the present analyses should unavoidably unravel shortcomings of the potential, whether regarding interactions in the Zn(II) cores or those of the arms with the periphery. These should enable to refine the strategy for the next stage of SIBFA calibration to be resumed at the correlated level. It would likely be hopeless to undertake large-scale MD/FEP simulations if shortcomings already at the HF level were not identified beforehand.

While in the present study ΔE(SIBFA) was shown to reproduce in consistent fashion the trends of ΔE(QC) in the above-mentioned cases a-e, it overestimated it after accounting for BSSE and the relative energy differences between the five inhibitors left room for improvement. This led us to revisit the parameters of TZT, of the benzocarboxylate arm and of imidazole, upon resorting to the LSQF procedure using a Zn(II) probe approaching these ligands in-plane as well as perpendicular to the plane as detailed below.

The first series of subsequent evaluations bear on the two mono-zinc cores and the dizinc core, whether TZT-uncomplexed or TZT-complexed, as extracted from the optimized complex of VIM-2 with each inhibitor. There is thus a total of thirty complexes on which ΔE(SIBFA) and ΔE(HF) are done in parallel. This enables to probe the 'flexibility' of the dizinc core anchoring TZT because it can partly distort to allow optimizing the interactions of the arms with the periphery: how well could such a flexibility be reflected by ΔE(SIBFA) and its contributions as compared to the HF ones?

The five complexes a-e) are then reconsidered with the extended recognition site to evaluate the amount of improvement now realized.

Additional validations bear, for each inhibitor, on the compared ΔE(SIBFA) and ΔE (QC) values and of their contributions on the complexes of each arm with its VIM-2 interacting partners. These interactions are either ionic, polar, cation-π, or π-stacking.

We finally provide ALMOEDA results on the mono-and dizinc sites with two DFT functionals, ωB97X-D[46] and B3LYP-D3 [47]. This enables to unravel the impact of correlation/dispersion on each separate QC contribution and how well could ΔE(SIBFA) with correlated multipoles and polarizabilities and augmented with dispersion match the QC results prior to any further refinement, whence an upper bound to the expectable error.

We believe the interest of such analyses should extend far beyond the targeting of MBLs, notwithstanding their essential importance as targets for drug development. Thus Zn-metalloproteins when overexpressed are responsible for numerous diseases, with very few efficient inhibitors at this time.

Although this list is far from exhaustive, newly-emerging targets are matrix metalloproteinases (MMP), involved in matrix invasion and metastases [48,49], neural inflammation [50] and auto-immune diseases [51], histone deacetylase (HDAC), involved in cancer [52], and phosphomannose isomerase (PMI) in microbial and parasitic diseases [53].

Computational procedure.

Ab initio QC.
The computations used the aug-cc-pVTZ(-f) and cc-pVTZ(-f) basis sets [54, 55].
The complexes of the five inhibitors with the extended recognition site were computed with the G09 software [56] and included the Basis Set Superposition Error (BSSE [57]) correction.
Energy Decomposition Analyses (EDA) at the HF level were done with the Reduced Variation Space Analysis by Stevens and Fink [38] coded in the GAMESS [58] software. The DFT computations were done with the B3LYP-D3 [47, 59] and the ω-B97X-D functionals [46]. EDAs at the DFT levels were done with the ALMOEDA procedure [39] coded in the Q-Chem software [60].

Polarizable Molecular Mechanics (PMM). The PMM computations were done with the SIBFA procedure [4]. The intermolecular interaction energy, ΔE, is computed as a sum of five contributions: electrostatic multipolar (E_{MTP}), short-range repulsion (E_{rep}), polarization (E_{pol}), charge-transfer (E_{ct}) and dispersion (E_{disp}). Their expressions were detailed in several previous papers [4, 13, 15]. The distributed multipoles on the fragments making up VIM-2 (backbone and side-chains) and the inhibitors (TZT and its substituents on the R1 and R2 sites) were obtained by the Generalized Distributed Multipole Analysis (GDMA) by Stone [61] with the aug-cc-pVTZ(-f) basis set. The distributed polarizabilities, located on the bond barycenters and the extremities of the heteroatom lone-

pairs were derived from the Garmer and Stevens procedure [62] coded in GAMESS.

We have resorted to the X-ray structure of the complex of VIM-2 with inhibitor JMV4690 [pdb code 6YRP, Ref. 34] as a starting point for energy-minimizations (EM) of the five complexes. These resorted to the Merlin software [63]. As in our previous studies [25-27], the protein backbone was held rigid. We relaxed the protein side-chains around their χ torsional angles. The six intermolecular variables defining the orientation of the inhibitors and their torsional angles were minimized. Fourteen 'discrete' water molecules were retained for each complex, based on proximity criteria and their six intermolecular variables were minimized. The intramolecular bond lengths and valence angles were not relaxed. At the outcome of the EMs, the comparisons between SIBFA and QC were on an extended recognition site of VIM2. Such sites, in addition to the entirety of the inhibitors and to the dizinc binding site, encompassed all VIM-2 residues (backbone and/or side-chains) interacting with the inhibitors, as well as the fourteen discrete waters. The same residues were retained in all five complexes:
backbone atoms of Cys-221, Tyr224-Glu225; Gly232-Val234; side-chains of Tyr67, Ser69, Trp87, His116, His118, Asp119, Asp120, Arg121, His196, Cys-221, Tyr224, Glu225, Arg228, Asn233, His263.

Refinements of the TZT, benzocarboxylate, and imidazole fragments.
In light of the comparisons with the QC results on the extended recognition site, we sought for further refinements of the relevant parameters for TZT, for the benzocarboxylate arm (an R2 substituent in four of the five considered inhibitors), but also for imidazole, which occurs four times out of six as a Zn-ligand in the dizinc binding core of VIM-2. We have resorted to a procedure recently integrated into the standard SIBFA software and used to calibrate the dianionic phosphate group (DPG) [64] and to derive a water potential grounded on Symmetry Adapted Perturbation Theory [SAPT] for molecular dynamics simulations on liquid water [Naseem-Khan et al., to be submitted]. The relevant fragment specific parameters for the SIBFA E_{MTP}, E_{rep}, E_{pol} and E_{ct} contributions were optimized by Least-Squares Fit minimization of the error with respect to their respective RVS counterparts E_C, E_X, E_{pol} and E_{ct} as computed in all probed positions of the fragment. Minimization was done with a BFGS procedure with numerically-computed gradients [65].

TZT was 'probed' by Zn(II) along both deprotonated ring nitrogens and sulfur upon performing distance and in- and out-of-plane angular variations. The five ring atoms were also probed vertically, upon performing distance variations along the perpendicular passing through the probed atom. In order to ensure better control of the non-additivity of E_{pol}, we have included in the optimization procedure the ten complexes of TZT with the monozinc cores, that is, each of the His3 and Asp-Cys-His cores in their structures extracted from their complexes with each of the five inhibitors. As in previous studies [33, 64], we have similarly resorted to a Zn(II) 'probe' to maximize the response of the probed ligands regarding both first-order (Coulomb and exchange), and second-order (polarization and charge-transfer) responses. Thus benzocarboxylate was probed by Zn(II) approaching one anionic carboxylate upon performing in-plane radial and angular variations, and radial variations along a perpendicular to the plane passing through this oxygen, or to the extracyclic C atom or the C atoms *ortho*, para or meta to it. Imidazole was probed by radial variations of the approach of Zn(II) along the external bisector of its deprotonated nitrogen. At equilibrium distance (1.90 Å) out-of-plane variations were

done until the perpendicular to the ring was reached. To improve the control of non-additivity, we included the five complexes of Zn(II) in the His3-monozinc core in its energy-minimized structure with the five inhibitors.

Results and discussion.

1. Complexes of inhibitors I-V with the extended recognition site. Starting validations.

The structures of the complexes of the five inhibitors with the extended binding sites are shown in Figures 2(a-e). In the first monozinc binding site, Zn(II) is bound to three His residues (His116, His118 and His196) and the partially anionic ring TZT N^2 atom *ortho* to the extracyclic S. In the second site, the other Zn(II) is bound by one Asp (Asp120), one Cys (Cys221), and one His residue (His263), and by the extracyclic TZT S atom. For convenience, we will denote the two Zn-sites as the 'blue' and the 'colored' site, respectively. The most relevant interatomic distances are listed in Supp. Info 1. It is seen that the distances of each Zn-atom to its ligands can vary by up to 0.2 Å. For conciseness, we will use an alternative notation for ligands 4690, 4390, 4684, 5064 and 5069, namely I-V, respectively.
The interactions occurring with the R1 arm, which substitutes the TZT C^5 atom involve the side-chains of residues Phe61, Trp87, and Asp119. Those occurring with the R2 arm, which substitutes the N^4-hydrazone involve the side-chains of residues Arg228, His263 and the main-chain atoms of residues Glu225 or Asn233. They will be analyzed in section 6.

Single-point computations were done on the complexes of I-V with the extended recognition site, extracted from the energy-minimized complexes. As in our previous studies, the same geometries were used in the validation of QC and SIBFA computations. Table I compares the ΔE values in: the unligated sites a) without and b) with the fourteen water molecules; c) the sites complexed with the sole TZT anchor and without the waters; the sites complexed with the entire inhibitor d) without and e) with the waters.

For both complexes d) and e), ΔE(SIBFA) reproduces the ranking of ΔE(QC) affinities: I > II > IV > V >III. For the first three complexes, they are much closer to the BSSE-uncorrected ΔE(QC) values than to the uncorrected ones, with relative errors <0.5%. For the last two complexes, ΔE(SIBFA) is either closer to BSSE-corrected ΔE(QC) or intermediate between corrected and uncorrected ΔE(QC). As such, even though the ranking of the five complexes is accounted for, the ΔE(SIBFA) curve cannot parallel the ΔE(QC) curves, as illustrated in Figures 3a-b.

Another ΔE(QC) ordering is found for complexes c), involving the sole TZT anchor:
V > I > III > II > IV. It can also be accounted by ΔE(SIBFA), which has values intermediate between the uncorrected and corrected ΔE(QC) values. The relative errors are <2%. However, there are some undesirable features, notably the very small ΔE(SIBFA) values separating V from I, 1.9 kcal/mol out of 1230, compared to 17 in QC. The corresponding evolutions of ΔE(SIBFA) and ΔE(QC) are illustrated in Figure 3c.

In the absence of the TZT anchor, for complexes a without the waters, ΔE(SIBFA) reproduces ΔE(QC) with relative errors <1% at the BSSE-corrected level. At this stage, a reproduction of the ΔE(QC) ordering could no longer be ensured. Close

reproduction also obtains in the presence of the waters, the values of ΔE(SIBFA) being intermediate between the BSSE-corrected and uncorrected ΔE(QC) values.

The results for complexes c are revealing. They show the modulations of the affinities of the anchoring TZT group by the additional interactions of the inhibitor arms with their VIM-2 partners and the structural waters. This implies the need to account for such modulations as closely as possible in the context of ΔE(SIBFA), namely for complexes c, to prevent further imbalances with respect to ΔE(QC) when such interactions are embodied, as in complexes d and e. This led us to the next stage of this work: is it possible to narrow down the relative errors concerning the complexes of TZT in the two monozinc sites and the dizinc site in structures a-e?

2. Automated recalibration of the TZT anchor.

We denote throughout by E_1 the sum of first-order contributions, E_C and E_X in QC and E_{MTP} and E_{rep} in SIBFA, and by E_2 the sum of second-order contributions, E_{pol} and E_{ct}.

For all four contributions, the relevant parameters are the effective radii of TZT ring nitrogens and extracyclic sulfur. These values can differ as a function of the contribution. For E_{rep}, additional parameters are the internal variables defining the positions of the lone pairs with respect to their atom bearers, their occupation numbers, and the increment of effective radii along the lone pair directions. Related lone pairs, such as the pi ones on a given atom, or the sp^3-lone pairs of sulfur, are constrained to have the same values. For E_{ct} the additional parameters are the increments of corresponding effective radii. Regarding E_{pol}, and in the perspective of future MD simulations, the polarizability tensors were transformed into scalars, the values of which were taken as the average of the three diagonal elements. A multiplicative factor was used as an additional parameter for each scalar polarizability. Additional parameters are those concerning the Gaussian screening of the field undergone by TZT. Its original expression is given in Ref. [66]. There are four multiplicative factors: for the bond then the lone-pair polarizabilities prior to iterating, then for the bond and lone-pair polarizabilities upon iterating. To each is associated a value for the exponent of the Gaussian screening function. In the standard calibration which was performed manually in Ref. [33], all four multiplicative factors have the same values, and so do the four Gaussian exponents. To enable for more flexibility, and since we included the two mono-zinc cores in their five different geometries in the training set, all eight parameters were enabled to vary independently.
Figures 4(a-g) recast the compared QC(RVS) and SIBFA evolutions as a function of the probing position regarding: a) E_C and E_{MTP}; b) E_X and E_{rep}; c) E_{pol}; d) E_{ct}; e) E_1; f) E_2; g) ΔE. We report the selected 32 most relevant complexes of Zn(II):
1-5: in-plane binding to S, θ angle (C-S-Zn) at 105°, five 0.1 Å distance variations from 2.0 to 2.4 Å;
6-11: in-plane binding to S, Zn-S distance at 2.1 Å, six 30° θ angle variations from 60 to 240°;
12-15: binding to S, distance at 2.1 Å, θ angle at 105°, four 60° ϕ out-of-plane angular variations from 120° to 300°;
16-21: in-plane binding to N^2, *ortho* to the extracyclic sulfur, along its external bisector (θ angle of 126°), six 0.1 Å distance variations from 1.7 to 2.2 Å;
22-25: in-plane binding to N^2, distance at 1.8 Å, four 30° θ variations, from 66° to 156°;
26-32: in-plane binding to N^2, distance at 1.8 Å, θ at 126°, seven ϕ out-of-plane 30° angular variations from 90° to -90°.

To show control of the short-range repulsion in less relevant Zn(II) positions, we report for this contribution additional results with a more complete coverage of the volume around TZT:
33-36: in plane binding along the external bisector of the extracyclic hydrazone N;
37-61: approach along the perpendicular to TZT with distance variations from 1.8 Å till 2.2 Å. *37-41* are to N^1, *meta* to the sulfur, 42-46 to N^2, *47-51* to C, *52-56* to the substituted N, and *57-61* to the extracyclic N.
62-67: in-plane binding to N^1 along its external bisector, distance variations from1.7 to 2.2 Å;
68, 69 and 70: in-plane binding to N^1, distance of 1.8 Å, θ angles of 96°, 156°, and 186°.
The LSQF-optimized SIBFA TZT parameters for E_{MTP}, E_{rep}, E_{pol} and E_{ct} are given in Supplementary Information S2.

The largest relative error of E_{MTP} with respect to E_C is 6%, occurring for in-plane binding to N^2 at a distance of 1.8 Å to N^2 (Figure 4a, position *25*).
The closest QC reproductions are those of E_X(RVS) by E_{rep}(SIBFA) over the 70 probe positions (Figure 4b).
Those concerning E_{pol} (Figure 4c) are at positions *1-3,* for the three shortest distances of approach to S (2.0-2.2 Å), and at position *12*, where Zn(II) binds TZT out-of plane.
The least regular matches concern E_{ct} (Figure 4d). Positions *1-5* and *16-20* relate to the variations of the distances of Zn(II) to S and N^2, respectively: E_{ct}(SIBFA) undergoes faster variations than E_{ct}(RVS), which is much shallower and could actually start to increase in magnitude past the reported distances. It was earlier reported that in monoligated complexes of Zn(II) [66, 67] and lanthanides [68] such an increase in magnitude upon increasing distance is caused by the admixture of a state with transfer of a 'complete' electron from the ligand to the cation [69]. This is prevented in polyligated Zn(II) complexes. In positions *26-32*, the underestimated values of E_{ct}(SIBFA) are compensated for by E_{pol}(SIBFA) within E_2 (Figure 4f).
The lowest-energy position is *22* (Figure 4g) for which Zn(II) bridges N^2 and N^1 at distances of 1.8 and 1.7 Å, respectively. The second minimum is at position *25*, for in-plane binding to N^2 with a θ angle of 156°, for which Zn(II) bridges N^2 and S, at distances of 1.8 and 2.5 Å respectively. ΔE(SIBFA) is overestimated by 5%, due to E_{MTP}. The largest overestimation of ΔE is in the fifth second minimum (position *7)* in which Zn(II) binds in-plane S at an angle of 2.1 Å, and it is caused by E_{pol}.
These results imply that further refinements to E_{pol} could be considered at a later stage, such as by enabling a relaxation of the internal coordinates defining the position of each centroid with respect to its bearer, in addition to the actual modulation of the amplitude of the polarizability. On the other hand, the strong reduction of the magnitudes of E_{pol} and E_{ct} in polyligated Zn(II) complexes due to anti-cooperativity could limit the impact of the shortcomings occurring in monoligated complexes. How well could then ΔE(SIBFA) and its contributions fare in the two monozinc cores and the dizinc core of VIM-2, whether uncomplexed or complexed by TZT?

3. Mono-zinc binding cores in geometries I-V.

Tables II(a-d) compare ΔE(SIBFA) and ΔE (QC) for each mono-zinc binding core, extracted from the VIM-2 complexes with the five inhibitors in four distinct cases: a) the 'blue' and b) the 'colored' core uncomplexed by TZT; c) and d) the 'blue' and 'colored' cores complexed by TZT, respectively. They are commented in succession.

a). 'Blue core'. ΔE(SIBFA) retains values reproducing ΔE(QC) to within 3 kcal/mol out of 300, i.e. relative errors < 1.5%. I-IV have ΔE values themselves differing by <1.5%. On the other hand, ΔE(SIBFA) in V is less stabilizing by 6 kcal/mol, and this is consistent with ΔE(QC). For all five complexes, E_1 has a lesser magnitude than E2 with both approaches. With both as well, the largest E_2 versus E1 magnitudes are with IV, while it is in I that E_1 comes closer to E_2. E_1(SIBFA) comes very close to E_1(QC) (less than 1 kcal/mol out of 150) but there are error compensations, E_{MTP} having larger magnitudes than E_C, while conversely E_{rep} is smaller than E_X.

b) 'Colored core'. ΔE(SIBFA) retains a very close numerical agreement with ΔE(QC), with 1% relative errors, for all five cores. The two best bound cores are those of II and IV. Both E_1 and E_2 are closely reproduced as well. Again, there are compensations of errors coming into play within E_1, but this time it is E_{MTP} that is smaller in magnitude than E_C, E_{rep} now being smaller than E_X. E_2 is now more than three times smaller in magnitude than E_1, in marked contrast to the situation occurring in the blue cores a. This translates the very strong anti-cooperativity of E_{pol} and E_{ct}, owing to the presence of two anionic ligands, overcompensating for their stronger polarizabilities and electron-donating characters. Of note is, with both QC and SIBFA, the rather modest increases of the magnitude of E_{ct} upon passing from the 'blue' cores (all neutral imidazole ligands) to the 'colored' ones, despite these having two anionic ligands with much smaller ionization potentials and much more extended electronic clouds than imidazole.

c). TZT-complexed blue core. ΔE(SIBFA) retains a close agreement with ΔE(QC) upon TZT binding to the 'blue' core. The ranking I > III > II > V > IV is the same as that of ΔE(QC), but this could be coincidental given the very small differences between the complexes: there are very small relative errors of ΔE(SIBFA) with respect to ΔE(QC) of 1%, but with one notable exception, V, the least favored complex, for which the relative error is 3%: this is the largest relative error among all the twenty considered *a-d* mono-zinc complexes in structures I-V. It is mostly due to E_{pol}(SIBFA), which is 7 kcal/mol out of 130-140 smaller in magnitude than E_{pol}(QC), while it retained very close values to it in the four other complexes. In line with a conclusion from the above-reported monoligated study, a finer tuning of E_{pol}(SIBFA) in polyligated complexes would likely be enabled by additional LSQF relaxing the three internal variables (the distance and the θ and ϕ angles), which define the position of each polarizability with respect to their bearer, atom or barycenter, as was done for the lone-pairs regarding E_{rep}.
E_{ct}(SIBFA) closely follows the evolutions of E_{ct}(QC) but is underestimated by a difference of 6-8 kcal/mol with respect to it. E_1(SIBFA) has a noteworthy agreement with E_1(HF), and so do both E_{MTP} and E_{rep} compared to E_C and E_X. Small overestimations of E_1(SIBFA) can 'absorb' to some extent the corresponding underestimations of E_{ct}. It is instructive to compare for each complex I-V the values of E_{pol} and E_{ct} prior to, and following, complexation by TZT. We observe very modest increases of their magnitudes following complexation, and much more so in the case of E_{ct}. For both contributions, this reflects the strong inhibition by anti-cooperativity of the contribution of TZT to E_2, opposing its polarizability and electron-donating properties.

d). Complexed colored core. ΔE(SIBFA) retains very close numerical agreements with ΔE(QC) throughout, the largest relative error being 2.3% for complex III. E_1(SIBFA) has by up to 2% larger magnitudes than E_1(QC), due mostly to E_{MTP} but this is compensated by smaller magnitudes of E_2(SIBFA) than E_2(QC). It is instructive, here also, to compare the separate evolutions of E_{pol} and E_{ct} upon passing from the

uncomplexed to the complexed 'colored' core, namely complexes *b* and *d*. E_{pol}(QC) and E_{ct}(QC) increase by limited amounts, by about 9 and 8 kcal/mol respectively. A notable exception is complex V, where E_{pol}(QC) has *diminished* in magnitude, albeit by a small amount (2 kcal/mol out of 95) and E_{ct}(QC) has increased in magnitude by half the amount observed in I-IV. Both trends are seen in SIBFA for V. While for I-IV the magnitude increases of E_{ct}(SIBFA) of 7 kcal/mol are very close to those of E_{ct}(QC), the corresponding increases of E_{pol}(SIBFA) are much smaller (<2 kcal/mol) with even a small decrease in magnitude for IV. In retrospect, this suggests that a similar LSQF fine-tuning of the E_{pol} parameters for formate and methanethiolate should be envisaged as done for imidazole, encompassing polyligated complexes in the training set. This will also be considered in forthcoming refinements at the correlated level. At this stage it could be noted that the present close reproduction of the QC values might exempt from this extra endeavor at this stage.

4. Dizinc binding cores in geometries I-V.

Tables III(a-b) report the BSSE-corrected ΔE(QC) and ΔE(SIBFA) values in the dizinc core, uncomplexed (a) and complexed (b) by TZT. RVS analyses could not be performed for size reasons. We have resorted to QC calculations with both aug-cc-pVTZ(-f) and cc-pVTZ(-f) basis sets.

a) Uncomplexed cores.
There is a very striking agreement of ΔE(SIBFA) and ΔE(QC), actually better with the aug-cc-pVTZ(-f) basis set, the relative errors being <1%. To some extent, it stems from mutual compensations from the separate mono-zinc cores, since ΔE(SIBFA) was found to smaller and larger magnitudes than DE(HF) in the blue and the colored cores, respectively.

b) TZT-complexed cores.
ΔE(SIBFA) remains able to reproduce ΔE(QC) with relative errors <1%. Such accuracy was far from granted at the outset. Given the small magnitude of such an error, it would be illusory, here again, to compare the rankings of the ΔE values in the five complexes. A preference in favor of complex V nevertheless emerges from both ΔE(QC) and ΔE(SIBFA). Complex IV is the one with the least ΔE(SIBFA) versus ΔE(QC) stabilization. This can be traced back again to the outcome from complex IV in the colored mono-zinc core, the relative underestimation mostly stemming from E_{pol}(SIBFA) in this complex. This was discussed in paragraph 3 above with possible means towards a finer tune-up. It provides an illustration of the insight afforded by EDAs in a segmental approach.

5. Reconsidered complexes of inhibitors I-V with the extended recognition site.

Table IV recasts the results of the first section of this study, starting with the TZT-uncomplexed cores within the extended VIM-2 recognition site (a) and ending up with the complexes of the entirety of ligands I-V with the site, without (d) and with (e) the water molecules. For the complexes of the TZT anchor with site (c) as well as those of the entirety of the ligand (c and d), ΔE(SIBFA) has come closer numerically to BSSE-corrected ΔE(QC) than at the outset, as can be seen by comparing Tables I and IV. There remains an exception, that of TZT in complex IV, for which ΔE(SIBFA) has a smaller (by 0.6%) value than ΔE(QC). Again, this can be traced back to the situation with its complex with the 'blue' site in this very structure IV, identifying E_{pol} as the cause for the underestimation. The compared evolutions of ΔE(SIBFA) and

ΔE(QC) in complexes c, d and e are reported in Figures 5a-c. A significant improvement of the shape of ΔE(SIBFA) curve relative to ΔE(QC) is visible in Figures 5b-c, as compared to Figures 3b-c.

6. Separate interactions of the two arms with VIM-2 residues around the dizinc binding site.

We have further considered the complexes of R1 and R2 arms with their interacting partners. These are of four types: ionic, H-bonding, π-stacking and cation-π. How well, prior to any recalibration than that of imidazole and benzocarboxylate, could ΔE(SIBFA) and its contributions match the ΔE(QC) results? The results are reported in Tables Va-e regarding ligands I-V.

Ligand I (4690). The benzocarboxylate arm interacts with its ring perpendicular to the Arg228 side-chain, and *oblique* to the Tyr67 side-chain. In both cases ΔE(SIBFA) can match ΔE(QC). Of note are the very strong stabilization energies of the Arg228 complex, even though the extracyclic carboxylate does not directly interact. ΔE has positive values with the neutral Tyr67 side-chain owing to the absence of dispersion/correlation, an accurate SIBFA calibration which is planned as a next stage in light of SAPT analyses. Lesser accuracy is observed with the His263 side-chain, with which a parallel stacked arrangement takes place, and with the Asn233 main-chain, with the carboxylate group as a proton acceptor from the amino group. These are, rather surprisingly, mainly caused by E_{MTP} in both cases. This could possibly be due to the calibration of the parameters of its penetration component (reported in Ref. 43), in which the charge-quadrupole component was given a negligible weight. This is presently being reconsidered in the context of SAPT recalibration with correlated multipoles, and it will be instructive to reconsider this issue when this is completed in turn. Related overestimations with His263 side-chain and VIM-2 backbones are also encountered with the other ligands (see below).
The R1 substituent interacts with its ring perpendicular to the Phe61 side-chain, and oblique to the Trp87 one, with an H-bond interaction taking place between the extracyclic methoxy group and the Trp87 imino nitrogen. Overestimations of E_{MTP} could again be noted. Such complexes might thus also have to be reevaluated with SAPT.

Ligand II (4390). Similar remarks are found as with ligand I, the geometries of the two complexes being closely related: regarding benzocarboxylate, close ΔE(SIBFA) and ΔE(QC) values for Arg228, overestimated E_{MTP} values with His263 side-chain and Asn233 main-chain, as well as regarding the interactions of R1 with Phe61 and Trp87 side-chains.

Ligand III (4684). The N-hydrazone-connected 2,4-dihydroxy-phenyl group interacts with Arg228 by an H-bond between its para-hydroxyl oxygen and one Arg228 amino group (dO-H=2.29 Å). It has its ring perpendicular to the Tyr36 ring and nearly parallel to that of His263. ΔE(SIBFA) matches well ΔE(QC) but there are again E_{MTP} overestimations in the His263 complex, and to a lesser extent, in the Tyr67 one. E_{pol}(SIBFA) appears underestimated.
The C-connected 2,5-dihydroxy-phenyl group (substituent R1) has its meta-O hydroxyl accepting a proton from the imino group of Trp87 (dOH=2.05 Å) with its ring oblique to the indole and perpendicular to the Phe61 ring. E_{pol}(SIBFA) is underestimated, while E_{MTP} is overestimated regarding the interaction with Phe61. There is an overall acceptable match of ΔE(SIBFA) to ΔE(QC), pending the forecast refinements.

Ligand IV (5064). The interactions of the benzocarboxylate arm with Arg228 and His263 are similar to those found with ligands I and II, the best numerical agreement being with Arg228. As with these two ligands, the ΔE(SIBFA) values for its interaction with the Asn233 backbone are overestimated, again due to E_{MTP}.
The dichlorobenzene R1 arm interacts with Asp119 and Trp87 through one Cl substituent, acting simultaneously as an electron acceptor from Asp86 by its 'sigma hole' (dCl-O=2.86 Å) and as an H-bond acceptor from the imino proton of Trp56 (dCl-H=2.49 Å). It interacts in a near-perpendicular arrangement with Phe31 side-chain. Even though the summed ΔE(SIBFA) energies of R1 with the three side-chains are similar to the ΔE(QC) values (14.9 vs. 14.5 kcal/mol, respectively), improvements regarding its interaction with each residue appear necessary.

Ligand V (5069). The first phenyl ring of the R2 substituent interacts by perpendicular π-stacking with the Tyr67 side-chain, and simultaneously by a cation-π interaction with the Arg228 side-chain which binds perpendicular to it. As in the related π-stacking complexes with the other ligands, there are partial compensations between overestimated E_{MTP} and underestimated E_{pol} values.
The *m*-benzocarboxylate arm interacts with the main-chain of Glu225 and with the Arg228 and His263 side-chains. Its interaction with the Arg228 side-chain is much stronger than the one between the first phenyl ring and this residue, clearly due to the greater proximity of the carboxylate group and its greater overlap. It is noted that the summed ΔE(SIBFA) value of this ring with the Arg228 and His263 side-chains is the same (-40 kcal/mol) than that of ΔE(QC), but it is due to compensations between its under- and its overestimations with them, thus an additional incentive for further refinements of the aromatic entities.
The 2,5-dihydro-phenyl R1 arm binds in an oblique π-stacking arrangement to Trp87 with an additional H-bond of the *meta*-hydroxyl oxygen with the Trp87 imino proton (dOH=2.09 Å), with very close ΔE(SIBFA) and ΔE(QC) values. It also has a perpendicular π-stacking interaction with Phe61 side-chain.

7. Networks of structural waters.

There are tightly bound 'discrete' water molecules in the recognition site, which can either bind to both the ligand and protein residues, or mediate the interaction between them. They can be endowed with much higher dipole moments than liquid water [70-72], and possibly impact the ordering of relative affinities of ligands to a given target [70, 72]. For ligands I, II, and IV, we could identify related networks of discrete waters in the vicinity of their common benzocarboxylate arm and of its VIM-2 partners.

Thus, with the present notation, in the case of ligand I (4690), water *W1* donates one proton to one carboxylate oxygen and the other to the main-chain carbonyl of Asn233. It acts as an H-bond acceptor from the imino proton of His196, from the hydroxyl group of Tyr224 and from water *W2. W2* is in turn acceptor from the partly acidic H connected to the His263 C *ortho* to the Zn-binding nitrogen, and to *W3. W3* acts as an H-bond donor to the main-chain CO of Ile223, and as an H-bond acceptor from *W5. W5* acts as an acceptor from the main-chain NH of Glu225, and as a donor to *W4. W4* is also an acceptor from the imino cationic Arg228 side-chain and the partly acidic H belonging to the CH bond *meta* to the carboxylate, and acts as an H-bond donor to the anionic Glu225 side-chain. The simultaneous involvement of *W4* as an H-bond acceptor from a cationic side-chain and an H-bond donor to an anionic side-chain should explain its particularly large dipole moment of 2.94 Debye. With ligands II (4390) and IV (5064) the corresponding *W4* molecule is also the one with the largest dipole moment, namely 3.09 and 3.20 Debye, respectively.

A similar network is found in the high-resolution X-ray crystal structure of the VIM-2 complex with ligand I [34]. One water molecule does, related to *W4*, bridge the imino nitrogen of Arg228 and one anionic O of Glu225 (dON=3.10 Å; dOO=3.00 Å). It is H-bonded to a second water, related to *W5*, which is H-bonded to the main-chain N of Glu225, and to a third water, related to *W3*, bound to the main-chain O of Ile169. There is also one water, related to *W1*, which binds simultaneously to one O of the benzocarboxylate, to the hydroxyl of Tyr224 and the imino N of His196.
With ligand III (4684), devoid of an anionic *ortho* carboxylate, replaced by a hydroxyl group, a similar network could be observed as well, with *W4* having a value of 3.14 Debye.

A different network is observed with ligand V (5069), which has two phenyl rings at R2, with a *meta* carboxylate on the second one. *W1* accepts a proton from the main-chain NH of Asn233 and donates a proton to *W2* and the hydroxyl O of Tyr224. W2 donates a proton to one carboxylate O of R2 and to *W5. W5* donates a proton to this O as well, and to the main-chain O of Ile223. *W3* and *W4* donate a proton to one anionic O of Glu225 and to the other R2 carboxylate O, respectively. There are now three water molecules with large dipole moments, *W1, W2*, and *W5* with values of 2.63, 2.73 and 2.76 Debye, respectively.

8. Correlated ΔE calculations on the mono- and the dizinc cores.

It is essential to extend the present validations with advanced dispersion-augmented Density Functional Theory (DFT) functionals. This is a prime objective of SIBFA underway in the context of SAPT. But how close an agreement could be enabled at the present stage with DFT-D EDA's pending such refinements, could EDA enable to monitor the changes in the magnitude of each ΔE(QC) contribution upon passing from HF to DFT-D, and how well could their SIBFA counterparts account for such staged changes?

Table VI reports the ALMOEDA results on the blue and the colored mono-zinc binding sites with the B3LYP-D3 and the ω-B97X-D functionals using the cc-pVTZ basis set. We also report the corresponding SIBFA results with correlated multipoles and polarizabilities. We have used the same parametrization as in our previous study on the complexes of TZT with the zinc-binding cores of L1 [33]. The recalibration done in the present study for HF having resulted into a lesser agreement, was not retained. For comparison, we also report the ALMOEDA HF/cc-pVTZ results. Table VII reports the corresponding results on the dizinc core.

Blue Zn(II) core. E_1(ωB97X-D) is app. 7 kcal/mol larger in magnitude than E_1(B3LYP-D3) but E_2 is correspondingly 4 kcal/mol smaller with ωB97X-D, due essentially to E_{ct}. With both functionals, E2, which includes dispersion through the van der Waals kernel, has 30-35 kcal/mol larger magnitudes than E_1. E_1(HF) is smaller in magnitude than E_1(DFT-D), but this could result from a compensation between both large E_C and E_X values at the HF level. Most of the ΔE gains upon passing to the correlated levels stem from E_{pol} and E_{ct}, about 15 kcal/mol from both with the ωB97X-D functional.
E_1(SIBFA) has extremely close values to E_1(ωB97X-D), and follows consistent trends with it in the five complexes. Comparison with Table I shows that E_2(SIBFA) has comparable magnitudes than at the HF level, an increase in the magnitude of E_{pol} being compensated by a decrease of E_{ct}. The sum of E_2 and E_{disp}(SIBFA) follows very close trends with the five complexes as E_2(DFT-D). It has an approximately 5 kcal/mol out of 180 smaller magnitude than E_2(ωB97X-D) accounting for most of the

present underestimation of ΔE_{tot}(SIBFA). It reproduces the shallow behavior of ΔE(DFT-d) among complexes I-IV with variations of <1% and its decrease with complex V, due to E_2.

Colored Zn(II) core. E_1 now has extremely close values with both functionals, as well as with E_1(HF). E_1(SIBFA) has also very close values to E_1(QC) in complexes I-IV, the difference increasing, however, from <3 kcal/mol out of 460 to 7 kcal/mol out of 460, the corresponding relative error nevertheless remaining < 1.5%. E_2 has increased by app. 8 kcal/mol with respect to its values calibrated on HF results (Table I). The sum of E_2 and E_{disp} can now matches E_2(ωB97X-D) to within <6 kcal/mol out of 155, and evolves consistent to it in complexes I-V. Overall, ΔE_{tot}(SIBFA) can reproduce the numerical values of ΔE(ωB97X-D) very closely, the relative errors < 1.5%.

Binuclear Zn(II) core. E_1(ωB97X-D) has 15 kcal/mol larger magnitudes than E_1(B3LYP-D3) while E_2(ωB97X-D) has 10.5 kcal/mol smaller magnitudes than E_2(B3LYP-D3), resulting in only slightly larger magnitudes of ΔE(ωB97X-D) than ΔE(B3LYP-D3), of 3.5 kcal/mol out of 1000. The magnitude increase of DE upon passing from HF to DFT-d stems first from E_{ct}, about 40 and 50 kcal/mol with the ωB97X-D and B3LYP-D3 functionals, respectively, and then from E_{pol}, about 30 kcal/mol.
E_1(SIBFA) retains extremely close values to E_1(ωB97X-D), the relative errors not exceeding 1.2%. E_{pol}(SIBFA) is also close to E_{pol}(DFT-D), the relative errors < 3%. While as noted above, E_{ct}(SIBFA) is much smaller than its DFT counterparts, namely nearly one half, the inclusion of E_{disp}(SIBFA) results into a summed E_2 matching very closely the E_2(DFT-D) trends: its largest and smallest magnitudes are for complexes IV and V, respectively, with shallow variations in I-III. ΔE_{tot}(SIBFA) can match ΔE(DFT-D) with relative errors <2%. Figures 6a-c show the compared evolutions in complexes I-V of ωB97X-D and SIBFA for E_1, E_2 (including E_{disp} for SIBFA) and ΔE_{tot}, respectively. The trends are faithfully reproduced. We believe this is highly encouraging, considering that no extra calibration was attempted to match the DFT-D results at this stage.

Conclusions and Perspectives.

Zn(II) metalloproteins can be responsible for numerous severe pathologies, and are challenging targets for the design of novel efficient inhibitors, a need presently unmet. Among these are MBLs, responsible for the acquired resistance of bacteria against antibiotics which they cleave. In inhibitor-MBL complexes, the onset of very strong second-order polarization and charge-transfer precludes the use of 'classical' force-field simulations. Presently only QM/MM approaches could be safely considered, as well as semi-empirical approaches such as DFT-TB [23, 24]. But are these presently tractable to perform long-duration MD and free energy perturbation (FEP) calculations to derive free energies of binding, or could not, alternatively, polarizable MM be used as a surrogate to handle the inhibitor-MBL complex in its entirety?

In a previous study, we showed that the SIBFA procedure closely reproduced the values of ΔE(QC) and its individual contributions at play in the two separate mono-zinc cores and the dizinc core of two MBLs, L1 and VIM-2, both uncomplexed and complexed with a 1,2,4-triazole-3-thione (TZT) moiety, a conjugated monoanionic zinc-binding motif acting as an 'anchor' in the dizinc core. We have extended this study by now considering five TZT-containing inhibitors synthesized and tested in our

Laboratories. They have two arms, R1 and R2, substituting the TZT ring C^5- and extracyclic hydrazone, respectively. At the outcome of energy-minimization of their complexes with VIM-2, we have evaluated how closely could ΔE(SIBFA) reproduce ΔE(QC) in an extended recognition site made out of the dizinc core, the neighboring VIM-2 residues bound to each arm, and fourteen discrete waters. The interactions of these arms are of diverse nature, H-bonding, cation-π and π-stacking. ΔE(SIBFA) reproduced correctly the variations of ΔE(QC) along the series of the five complexes, and its numerical values. These were however overestimated, being closer to BSSE-uncorrected than to BSSE-corrected ΔE(QC), and the differences between some complexes were larger than the corresponding ΔE(QC) differences. Some of these could be traced back to the interactions of the sole TZT anchor in the five complexes, prior to including the contributions of the arms.

This issue led us to seek for refinements in its calibration. It was done by an automated procedure, which for each separate ΔE(SIBFA) contribution optimizes simultaneously the relevant parameters by LSQF minimizing its difference with respect to its ΔE(QC) counterpart for a diversity of TZT complexes with a Zn(II) cation probing in- and out-of-plane positions. This was extended to imidazole as well, because it is encountered as a Zn(II) ligand three times in the first mono-zinc core and once in the second. This enabled further refined reproductions of ΔE(QC) and its contributions by SIBFA. For each of the five structures derived from energy-minimization with each ligand, the validations were done on the two TZT-uncomplexed as well as on the TZT-complexed mono-zinc cores and dizinc core. This represents a total of thirty complexes, fifteen uncomplexed and fifteen complexed ones. With one exception, ΔE(SIBFA) could reproduce ΔE(QC) with a narrowed down relative error, now <1.5%. The 'outlier' had a relative error of 2.5%. The relative weights of E_1 and E_2 were correctly accounted for, thus attesting for a good control of non-additivity.

Retaining a good control is essential because any imbalance with respect to QC at this stage could result into an amplified imbalance when the arms are included, and into their suboptimal orientation in the extended site. The present calculations showed that the anchorage of TZT in the dizinc site retains flexibility, so that it is essential to be able to account for the sensitivity of ΔE(QC) and its contributions upon geometrical rearrangements, however limited.

We next revisited the complexes of the five inhibitors with the extended recognition VIM-2 site, totaling about 280 atoms. A significant improvement of the reproduction of ΔE(QC) was observed with respect to the starting situation, and this could be readily seen upon comparing the evolutions displayed in Figures 5a-c to those displayed in Figures 3a-c. It concerned a) the interactions of the sole TZT with the extended binding site; and the interaction of the entirety of the inhibitor b) prior to; and c) after the inclusion of the structured waters: in a) and b) ΔE(SIBFA) could match ΔE(QC/BSSE-corrected) with relative errors < 1.5% and an improved parallelism could be seen in all three cases. The relative errors were amplified to 2% in case c). This appears to be due to some overestimation of the contributions to DE of water. This should be remedied in the next phase of refinements, presently underway at the correlated level.

On the other hand, the interactions of the R1 and R2 arms with their VIM-2 partners showed that some improvements remained desirable, even if the remaining errors did not impair the overall agreements noted in stage b) above.

The above comparisons also gave clues for the future refinements that are being resumed, now at the correlated level:
-the calibration of the penetration component of E_{MTP} should give more weight to the charge-quadrupole term;
-the calibration of E_{rep} should be done upon resorting to an additional probe than Zn(II), such as water. This would enable for the response of its bond-bond and lone pair-lone pair components, as it is presently dominated by the lone pair-bond component, itself limited to an actual lone pair-atom component;
-the calibration of E_{pol} should allow for a partial relaxation of the internal coordinates of the polarizability tensors connecting them to their heteroatom or bond barycenter bearers.

We have extended the validations at the correlated level, regarding at this stage the unligated mono-zinc cores and the dizinc core. We resorted to the same calibration as in our previous work and performed EDA analyses with two advanced functionals, B3LYP and ωB97X-D. Close correlations were found in the fifteen complexes. E_1 was closely accounted for. The inclusion of E_{disp} enabled the sum of $E_{ct}+E_{pol}+E_{disp}$ to match the evolutions of the summed $E_{pol}+E_{ct}$ from ALMOEDA, in which the actual dispersion is included in the van der Waals kernel. There was a constant underestimation in the dizinc core of accountable for the present underestimation of ΔE_{tot}(SIBFA) with respect to ΔE(DFT/ωB97X-D), nevertheless limited to 2%.

The next stage of refinements is now starting, and should be reported subsequently. It resorts to SAPT-DFT on all protein and nucleic acid constitutive fragments, with Zn(II) and a dipolar molecule, water, probing a diversity of in-plane approaches, and perpendicular positions of conjugated fragments. SAPT delivers six separate contributions, including dispersion and exchange-dispersion, and their SIBFA counterparts should be able to match them by the LSQF approach, and, subsequently, more evolved approaches from applied mathematics. Other probes could be considered as well to enrich the diversity of the training set. Validations on multimolecular complexes will be done next, as in the present study, on multimolecular complexes using ALMOEDA and advanced DFT-D functionals.

We would like to reemphasize our essential motivation, namely long-duration MD on a series of drug-Zn-metalloprotein complexes, which should enable free energy perturbation studies delivering relative free energies of binding of competing inhibitors. Such studies are now rendered possible by very significant recent accelerations of the massively parallel Tinker-HP code [37]. The closer ΔE(SIBFA) to ΔE(QC) on the extended recognition sites, the safer the predictions of relative ΔGs on the complexes with the entirety of the protein.

Acknowledgments.
Part of this work was supported by the Agence Nationale de la Recherche (ANR-14-CE16-0028-01) including a post-doctoral fellowship to Dr. Kwapien. We wish to thank the Grand Equipement de Calcul Intensif (GENCI): Institut du Développement et des Ressources en Informatique (IDRIS), Centre Informatique de l'Enseignement Supérieur (CINES), France, project x-2009-07509, and the Centre Régional Informatique et d'Applications Numériques de Normandie (CRIANN), project 1990853.

Table captions.

Table I. Complexes of the extended recognition site of VIM-2 with ligands I-V. Compared ΔE(SIBFA) and ΔE(QC/HF) on the following:
a) intermolecular interactions prior to ligand binding and without the 'discrete' water molecules; b) intermolecular interactions prior to ligand binding and with the 'discrete' water molecules; c) intermolecular interactions with the TZT anchor and without the waters; d) intermolecular interactions with the entire ligands and without the waters; e) intermolecular interactions with the entire ligands and with the waters, Energies in kcal/mol.

Table II. Mono-zinc cores of VIM-2 in their complexes with the five inhibitors.
QC (HF/RVS) and SIBFA intermolecular interaction energies and their contributions. Energies in kcal/mol.

Table III. Di-zinc cores of VIM-2 in their geometries with the five inhibitors.
QC (HF/RVS) and SIBFA intermolecular interaction energies without and with the TZT anchor. Energies in kcal/mol.

Table IV. Complexes of the extended recognition site of VIM-2 with ligands I-V. Compared ΔE(SIBFA) and ΔE(QC/HF) at the outcome of the recalibration procedure on the following:
a) intermolecular interactions prior to ligand binding and without the 'discrete' water molecules; b) intermolecular interactions prior to ligand binding and with the 'discrete' water molecules; c) intermolecular interactions with the TZT anchor and without the waters; d) intermolecular interactions with the entire ligands and without the waters; e) intermolecular interactions with the entire ligands and with the waters, Energies in kcal/mol.

Tables V(a-e). Complexes of the R1 and R2 arms of ligands I-V with VIM-2 residues of the extended recognition site. Energies in kcal/mol.

Table VI. Compared ALMOEDA and SIBFA total interaction energies in the two mono-zinc binding sites. ALMOEDA results are at the B3LYP-D, ωB97X-D and HF levels. Energies in kcal/mol.

Table VII. Compared ALMOEDA and SIBFA total interaction energies in the dizinc binding sites. ALMOEDA results are at the B3LYP-D, ωB97X-D and HF levels. Energies in kcal/mol.

Figure captions.

Figures 1(a-e). Structural formulas of the five studied VIM-2 inhibitors

Figures 2(a-e). Representation of the energy-minimized complexes of the extended recognition site of VIM-2 with the five inhibitors.

Figures 3(a-c). Complexes of the extended VIM-2 recognition site with ligands I-V. Comparisons between ΔE(SIBFA) and ΔE(QC/HF) regarding: a) the entire ligand without the discrete waters; b) the entire ligand with the discrete waters; c) the sole TZT anchor.

Figures 4(a-g), Complexes of the TZT anchor with a probe Zn(II) ligand. Compared evolutions of SIBFA and QC/RVS ΔE contributions regarding: a) E_C and E_{MTP}; b) E_X and E_{rep}; c) E_{pol}; d) E_{ct}; e) E_1; f) E_2; g) DE.

Figures 5(a-c). Complexes of the extended VIM-2 recognition site with ligands I-V at the outcome of TZT, imidazole, and benzocarboxylate parameter refinements. Comparisons between ΔE(SIBFA) and ΔE(QC/HF) regarding: a) the entire ligand without the discrete waters; b) the entire ligand with the discrete waters; c) the sole TZT anchor.

Figures 6(a-c). Dizinc binding site. SIBFA and ωB97X-D/ALMOEDA intermolecular interaction energies prior to TZT binding. Compared evolutions in the structures of ligands I-V of: a) E_1; E_2 including E_{disp} for SIBFA; c) ΔE_{tot}(SIBFA) and ΔE(ωB97X-D).

Supporting information.

S1. List of Zn-TZT and ligand-VIM-2 distances in the complexes of the extended recognition site with ligands I-V.
S2. LSQF-optimized SIBFA TZT parameters for a) E_{MTP}; b) E_{rep}; c) E_{pol}; d) E_{ct}.

References.

1. L. Riccardi; V. Genna; M. De Vivo. *Nature Rev. Chem.,* **2018**, *2*, 100.

2. A. Y. Chen; R. N. Adamek; B. L. Dick; C. V. Credille; C. N. Morrison; S. M. Cohen. *Chem. Rev*. **2019**, *119*, 1323.

3. J. E. Raczynska; I. G. Shabalin; W. Minor; A. Wlodawer; M. Jaskolski. *Drug Resistance Updates* **2018,** *40,* 1.

4. N. Gresh; G. A. Cisneros; T. A. Darden; J.-P. Piquemal. *J. Chem. Theory Comput.* **2007**, *3,* 1960.

5. Y. Shi; Z. Xia; J. Zhang; R. Best; C. Wu; J. W. Ponder; P. Ren*. J. Chem. Theory Comput.* **2013,** *9,* 4046.

6. C. Liu; J.-P. Piquemal; P. Ren. *J. Chem. Theory Comput.* **2019,** *15*, 4122.

7. J.-P. Piquemal; G. A. Cisneros; P. Reinhardt, N. Gresh; T. A. Darden. *J. Chem. Phys.* **2006,** *124*, 104101.

8. R. Chaudret; N. Gresh; C. Narth ; L. Lagardere; T. A. Darden; G. A. Cisneros; J.-P. Piquemal. *J Phys. Chem. A.* **2014***, 118*, 7598.

9. O. Demerdash; Y. Mao; T. Liu; M. Head-Gordon; T. Head-Gordon. *J. Chem. Phys.* **2018,** *147,* 161721.

10. A. K. Das; L. Urban; I. Leven; M. Loipersberger; A. Aldossary; M. Head-Gordon; T. Head-Gordon. *J. Chem. Theory Comput.* **2019***; 15*, 5001.

11. G. Tiraboschi; B.-P. Roques ; N. Gresh *J. Comput. Chem.* **1999**, *20*, 1379–1390

12. G. Tiraboschi; N. Gresh; C. Giessner-Prettre; L. G. Pedersen; D. W. Deerfield. *J. Comput. Chem***. 2000**, *21*, 1011.

13. N. Gresh; J.-P. Piquemal; M. Krauss. *J. Comput. Chem.* **2005** *26*, 1113.

14. Z. Jing; R. Qi; C. Liu; P. Ren*. J. Chem. Phys.* **2017***, 147*, 161733.

15. L. El Khoury; S. Naseem-Khan; K. Kwapien; Z. Hobaika; R. G. Maroun; J.-P. Piquemal; N. Gresh. *J. Comput. Chem***. 2017**, *38*, 1897.

16. A. Warshel; M. Levitt. *J. Mol. Biol.* **1976***, 103*, 227.

17. T. Wesolowski; A. Warshel. *J. Phys. Chem.* **1994**; *98*, 5183.

18. J. Gao; M. Freindorf. *J. Phys. Chem. A* **1997***; 101*, 3182.

19. P. N. Day; J. H. Jensen; M. S. Gordon; S. P. Webb; W. J. Stevens; M. Krauss; D. R. Garmer; H. Basch; D. J. Cohen. J*. Chem. Phys.* **1996,** *105,* 1968.

20. I. Adamovic; M. A. Freitag; M. S. Gordon. *J. Chem. Phys.* **2003***, 118*, 6725.

21. M. S. Gordon; D. G. Fedorov; S. R. Pruitt; L. V. Slipchenko. *Chem. Rev.* **2012,** *112*, 632.

22. D. Loco; L. Lagardère; S. Caprasecca; F. Lipparini; B. Mennucci ; J.-P. Piquemal. *J. Chem. Theory Comput*. **2017***, 13,* 4025.

23. D. Xu; H. Guo; Q. Cui. *J. Phys. Chem. A***. 2007***, 111*, 5630.

24. Q. Cui. *J. Chem. Phys.* **2016,** *145*, 140901.

25. J. Antony; N. Gresh ; L. Olsen; L. Hemmingsen; C. J. Schofield; R. Bauer. J*. Comput. Chem.* **2002,** *23*, 1281.

26. J. Antony; J.-P. Piquemal; N. Gresh. *J. Comput. Chem.* **2005***, 26,* 1131.

27. N. Gresh; D. Perahia; B. de Courcy; J. Foret ; C. Roux; L. El Khoury ; J.-P. Piquemal. *J. Comput. Chem.* **2016***, 37,* 2770.

28. D. King; N. Strynadka. *Protein Sci.* **2011***, 20,* 1484.

29. J.-D. Docquier ; J. Lammotte-Brasseur ; M. Galleni ; G. Amicosante ; J.-M. Frere ; G. M. Rossolini. A*ntimicrob Chemother.* **2003,** *51,* 257

30. J. D. Docquier; S. Mangani*. Drug Resistance Updates* **2018,** *36,* 13.

31. M. F. Mojica; R. A. Bonomo; W. Fast*. Curr. Drug Targets* **2016***, 17,* 1029.

32. M. Makena; A. O. Düzgün; J. Brem, J.; M. A. McDonough; A. M. Rydzik; M. I. Abboud; A. Saral; A. C. Çiçek; C. Sandalli; C. Schofield, *Antimicrob. Agents Chemother.* **2016,** *60*, 1377.

33. K. Kwapien; M. Damergi, M.; S. Nader, S.; L. E Khoury; Z. Hobaika; R. G. Maroun; J. -P. Piquemal; L. Gavara; D. Berthomieu; J.-F. Hernandez; N. Gresh. *J. Phys. Chem. B.* **2017,** *121*, 6295.

34. L. Gavara; L. Sevaille; F. De Luca; P. Mercuri; C. Bebrone; G. Feller ; A. Legru; G. Cerboni; S. Tanfoni; D. Baud; G. Cutolo; B. Bestgen; G. Chelini; F. Verdirosa; F. Sannio; C. Pozzi; M. Benvenuti; K. Kwapien; M. Fischer; K. Becker; J.-M. Frère; S. Mangani; N. Gresh; D. Berthomieu; M. Galleni; J.-D. Docquier; J.-F. Hernandez, Eur. J. Med. Chem., under review.

35. J**.** Michel; J. W. Essex *J. Comput. Aided Mol. Des.* **2010,** *24*, 639.

36. J. Zhang; W. Yang; J.-P. Piquemal; P. Ren*. J. Chem. Theory Comput.* **2012***, 8,* 1314.

37. L. Lagardère; L.-H. Jolly; F. Lipparini; F. Aviat; B. Stamm; Z. F. Jing; M. H. Harger; H. Torabifard; G. A. Cisneros; M. J. Schnieders, M. J.; et al. *Chem. Sci.* **2018**, *9*, 956.

38. W. J. Stevens; W. Fink. *Chem. Phys. Letts,* **1987,** *39*, 15.

39. R. Z. Khaliullin; E. A. Cobar; R. C. Lochan' A. T. Bell; M. Head-Gordon*. J. Phys. Chem. A* **2007***, 111,* 8753.

40. B. Jeziorski; R. Moszynski; K. Szalewicz. *Chem. Rev.* **1994,** *94*, 1887.

41. A. J. Misquitta; B. Jeziorski; K. Szalewicz K. *Phys. Rev. Lett.* **2003,** *91*, 033201.

42. T. Dudev ; M. Devereux; M. Meuwly; C. Lim; J.-P. Piquemal; N. Gresh. *J. Comput. Chem.* **2015,** *36, 2*85.

43. M. Devereux; N. Gresh; J.-P. Piquemal; M. Meuwly. *J. Comput. Chem.* **2014***, 35,* 1577.

44. N. Gresh; J. E. Sponer; M. Devereux; K. Gkionis; B. de Courcy; J.-P. Piquemal; J. Sponer. *J. Phys. Chem. B.* **2015***, 119,* 9477.

45. N. Gresh; S. Naseem-Khan; L. Lagardère; J.-P. Piquemal; J. E. Sponer; J. Sponer. *J. Phys. Chem. B* **2017,** *121*, 3997.

46. N. Mardirossian; M. Head-Gordon*. Phys. Chem. Chem. Phys.* **2014,** *16*, 9904.

47. S. Grimme; J. Antony; S. Ehrlich; H. Krieg. *J. Chem. Phys.* **2010***, 132*, 154104.

48. C. Rouanet-Mehouas, B. Czarny, F. Beau, E. Cassar-Lajeunesse, E. A. Stura, V. Dive, L. Devel. *J. Med. Chem.* **2017***, 60*, 403.

49. B. L. Marcial ; S. F. Sousa ; I. L. Barbosa ; H. F. Dos Santos ; M. J. Ramos. *J. Phys. Chem. B* **2012**, *116*, 13644.

50. D. Leppert; R. L. P. Lindberg; L. Kappos; S. L. Leib. *Brain Research Rev.* **2001***; 36*, 249.

51. M. Ram; Y. Sherer ; Y. Shoenfeld*. J. Clin. Immunology* **2006;** *26*, 299.

52. N. J. Porter; D. W. Christianson. *Curr. Op. Struct. Biol.* **2019***,* *59,* 9.

53. L. Ahmad; S. Plancqueel; V. Dubosclard; N. Lazar; W. Ghattas; I. Li De La Sierra-Gallay; H. Van Tilbeurgh; L. Salmon. *FEBS Letts.* **2018**, *592*.

54. T. H. Dunning*. J. Chem. Phys.* **1989,** *90*, 1007.

55. D. Feller. *J. Comput. Chem.* **1996,** *17*, 1571.

56. M. J. Frisch; G. W. Trucks; H. B. Schlegel; G. E. Scuseria; M. A. Robb; J. R. Cheeseman; G. Scalmani; V. Barone; B. Mennucci; G. A. Petersson et al., Gaussian 09, Revision A.1, Gaussian Inc., Wallingford, CT, 2009.

57. S. F. Boys; F. Bernardi. *Mol. Phys.* **1970,** *19*, 553.

58. M. W. Schmidt; K. K. Baldridge; J. A. Boatz; S. T. Elbert; M. S. Gordon; J. H. Jensen; S. Koseki; N. Matsunaga; K. A. Nguyen; S. Su; T. L. Windus; M. Dupuis; J. A. Montgomery. *J. Comput. Chem.* **1993***, 14,* 1347.

59. L. Goerigk; S. Grimme. *Phys. Chem. Chem. Phys***. 2011***, 13,* 6670.

60. Q-Chem software (Y. Shao et al*., Mol. Phys***. 2015,** *113,* 184.

61. A. J. Stone. *J. Phys. Chem. A.* **2011,** *115,* 701,

62. D. R. Garmer; W. J. Stevens. *J. Phys. Chem*. **1989***, 93,* 8263.

63. G. A. Evangelakis; J. P. Rizos; I. E. Lagaris; I. N. Demetropoulos. *Comput. Phys. Commun.* **1987,** *46,* 401.

64. M. Devillers; J.-P. Piquemal; L. Salmon; N. Gresh. *J. Comput. Chem.* **2020,** *41,* 839.

65. The HSL Mathematical Software Library; Science and Technology Facilities

66. N. Gresh. *J. Comput. Chem.* ***1995,*** *16*, 856.

67. N. Gresh; D. R. Garmer. *J. Comput. Chem.* **1996,** *17,* 1481.

68. A. Marjolin; C. Gourlaouen; C. Clavaguera; N. Gresh; P. Ren; J. Wu; J.-P. Dognon; J.-P. Piquemal. *Theo. Chem. Acc.* **2012,** *131,* 1199.

69. G. Corongiu; E. Clementi. *J. Chem. Phys.* **1978,** *69,* 4885.

70. B. de Courcy; J.-P. Piquemal; C. Garbay; N. Gresh, *J. Am. Chem. Soc.* **2010***, 132*, 3312.

71. N. Gresh; K. El Hage; D. Perahia; J-P. Piquemal; C. Berthomieu; D. Berthomieu. *J. Comput. Chem.* **2014**, *35,* 2096.

72. N. Gresh; B. de Courcy; J.-P. Piquemal; J. Foret; S. Courtiol-Legourd; L. Salmon. *J. Phys. Chem. B* **2011,** *115*, 8304.

Figure 1

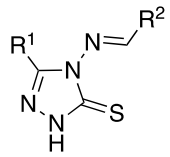

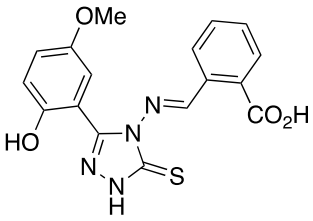

JMV4690 (I)

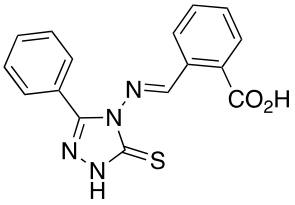

JMV4390 (II)

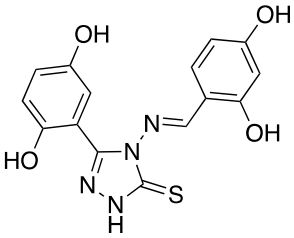

JMV4684 (III)

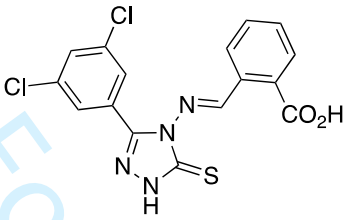

JMV5064 (IV)

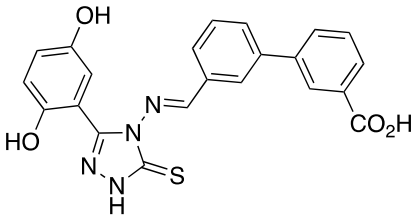

JMV5069 (V)

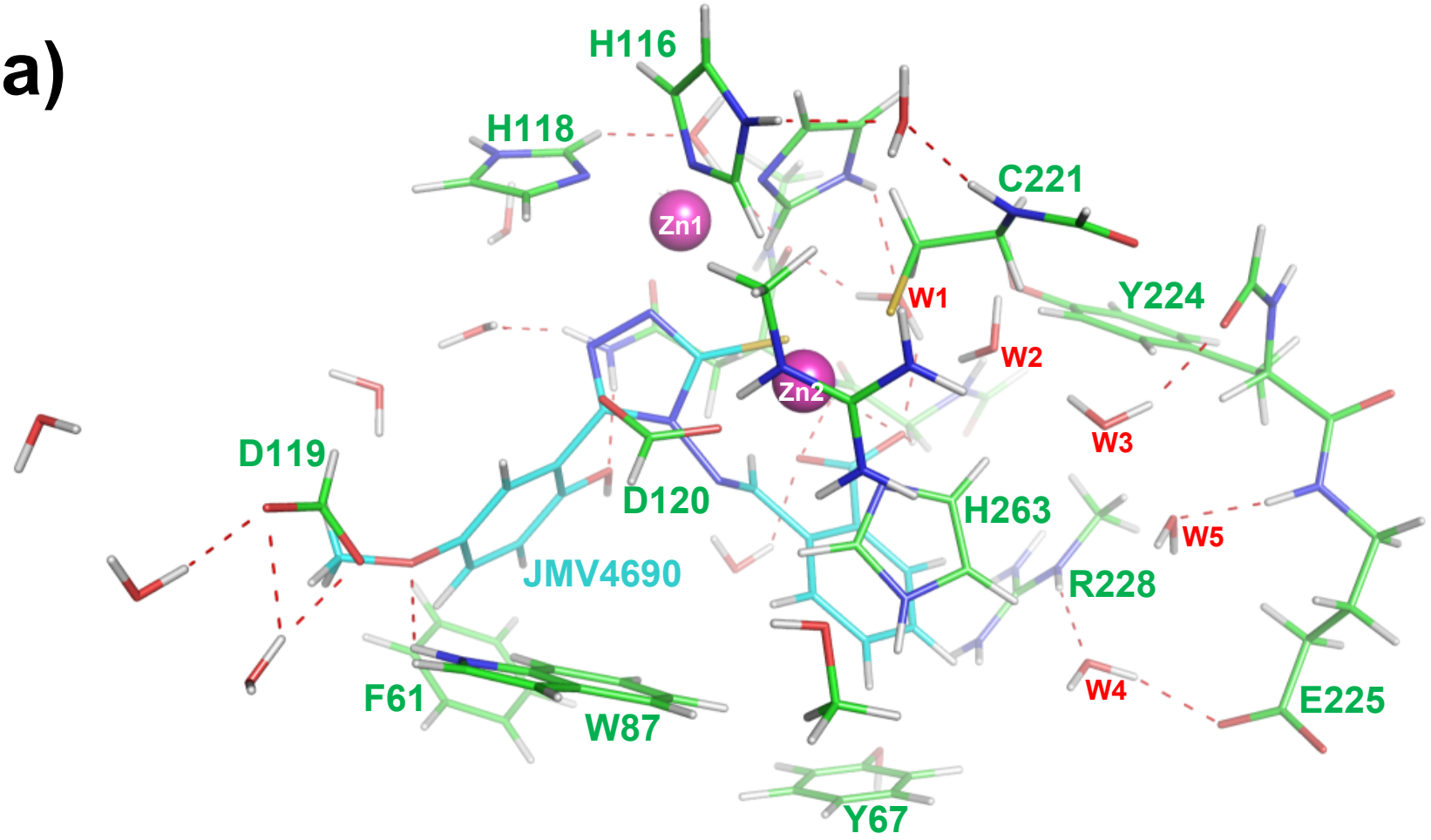
(a)
H116
H118
C221
Zn1
W1
Y224
W2
Zn2
W3
D119
D120
H263
W5
JMV4690
R228
F61
W87
W4
E225
Y67

(b)

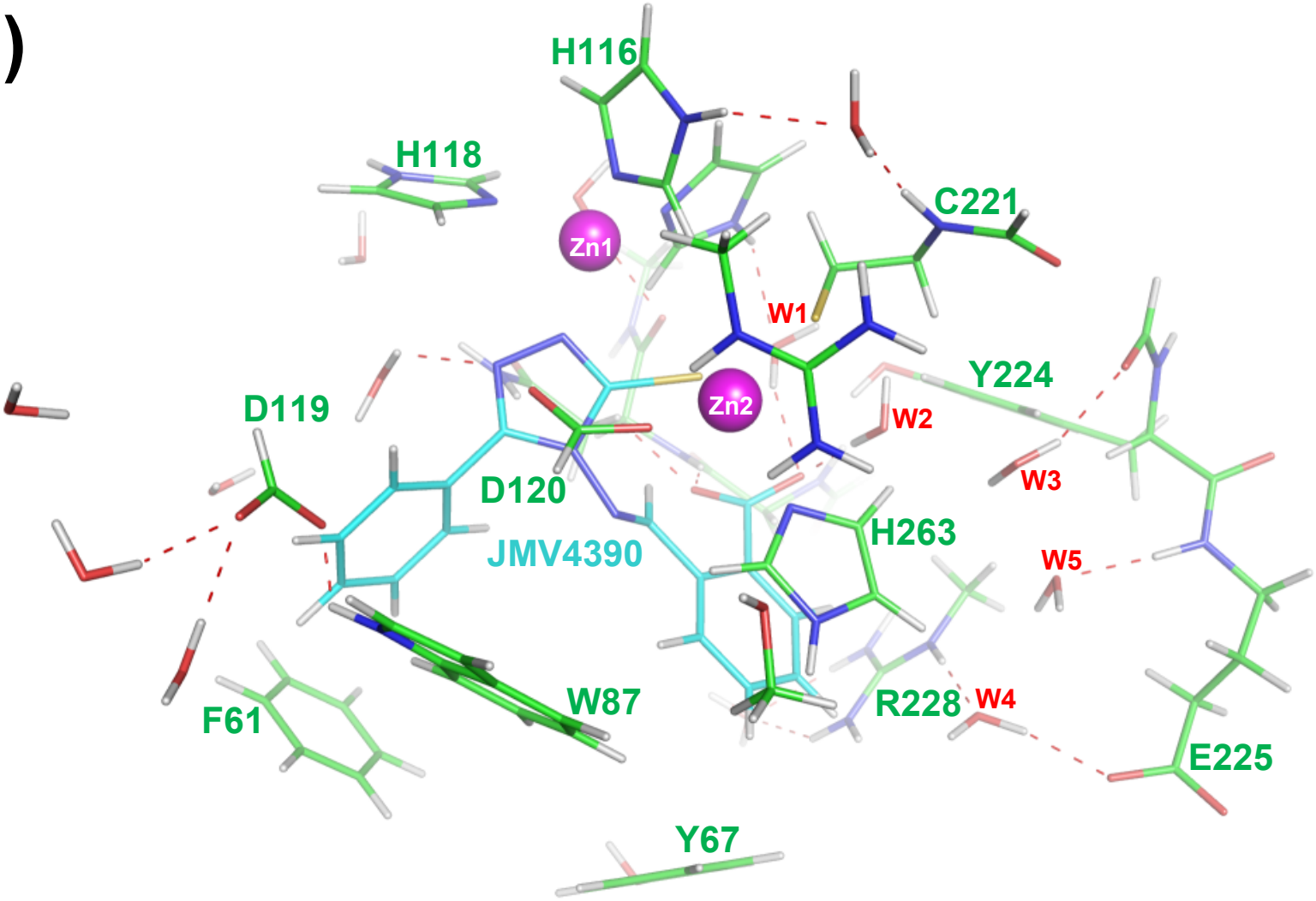

(c)

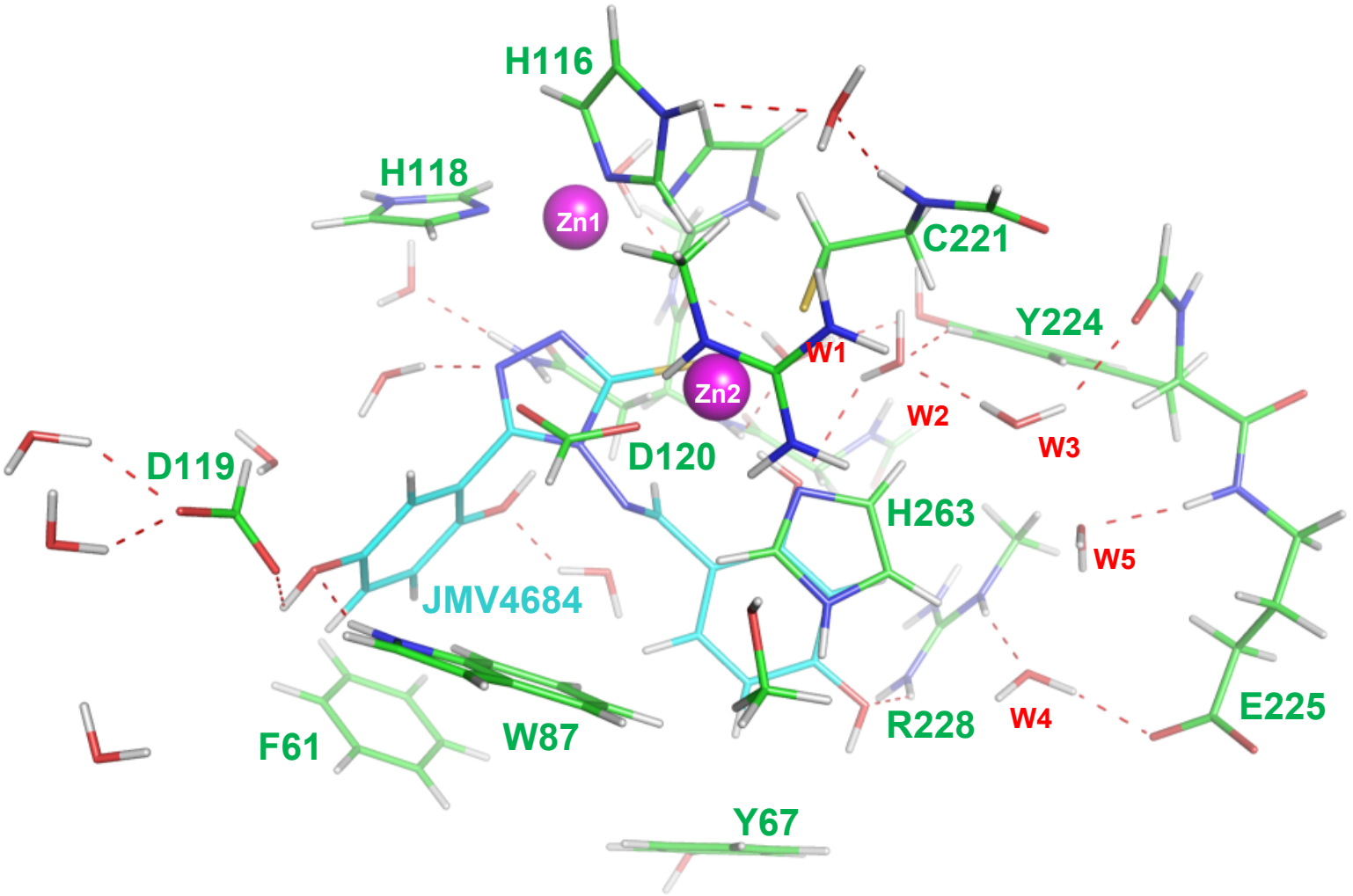

(d)

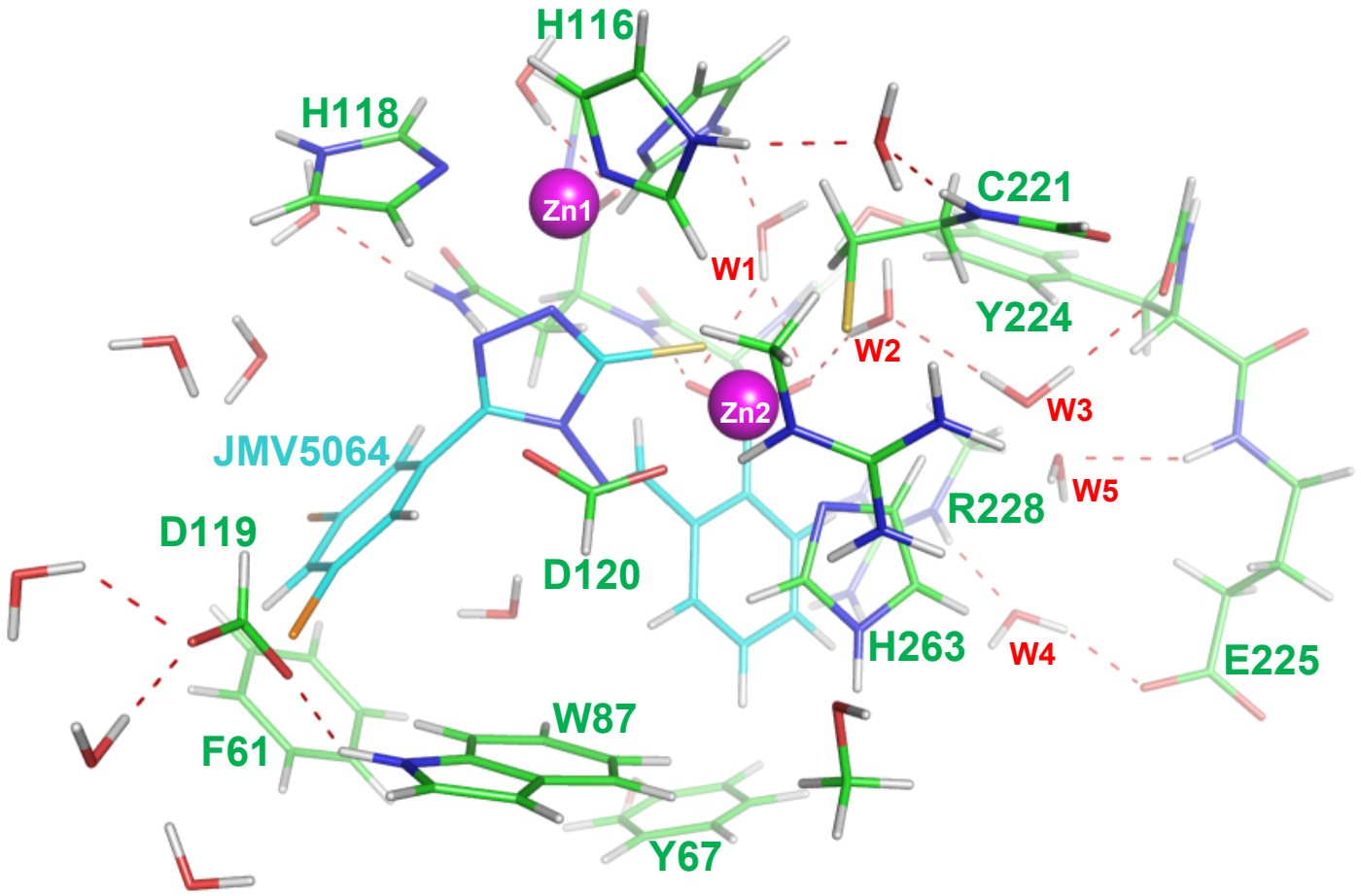
H116
H118
Zn1
C221
W1
Y224
W2
Zn2
W3
JMV5064
W5
R228
D119
D120
H263
W4
E225
W87
F61
Y67

(e)

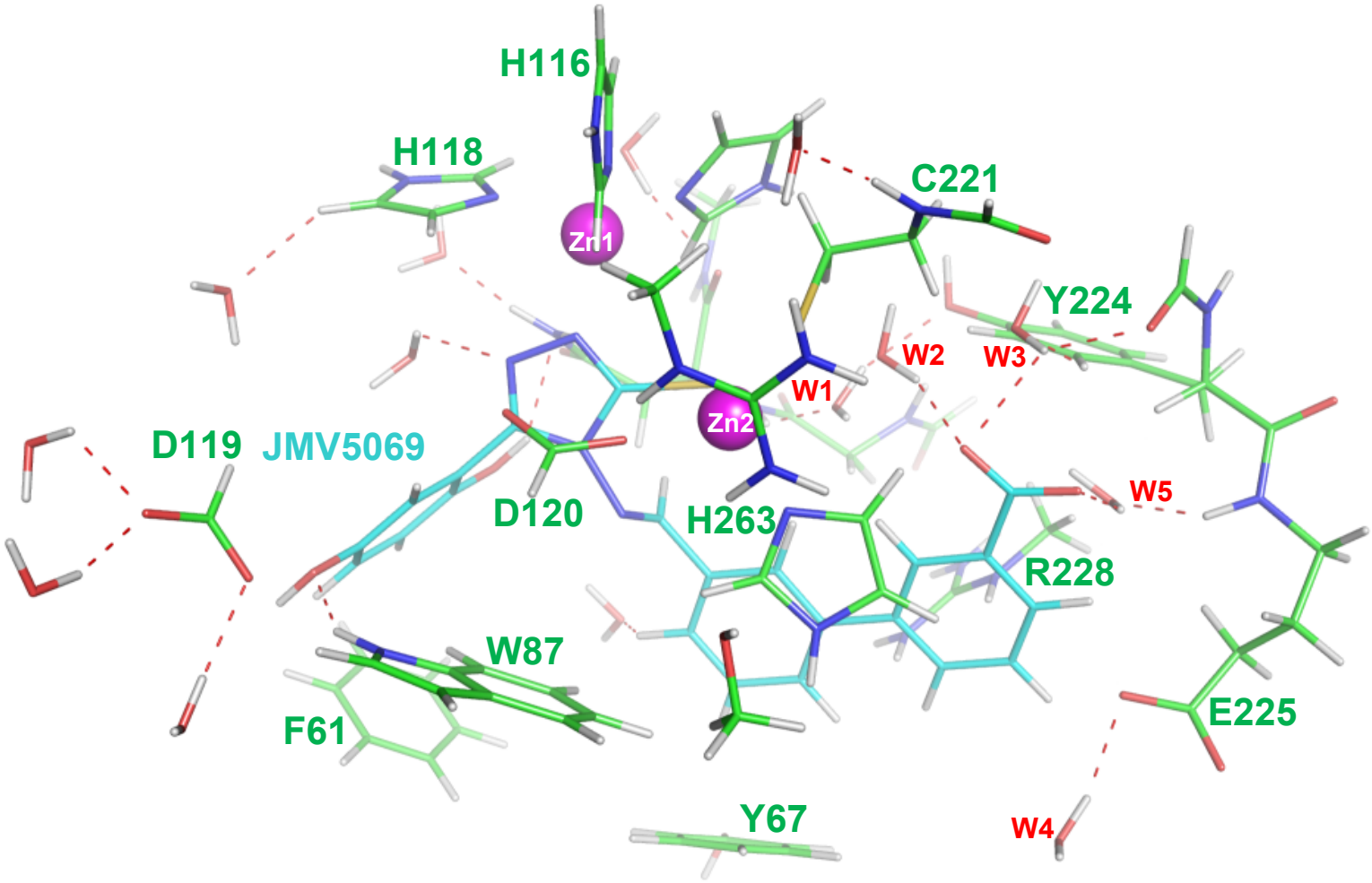
H116
H118
C221
Zn1
Y224
W2
W3
W1
Zn2
D119
JMV5069
D120
H263
W5
R228
W87
F61
E225
Y67
W4

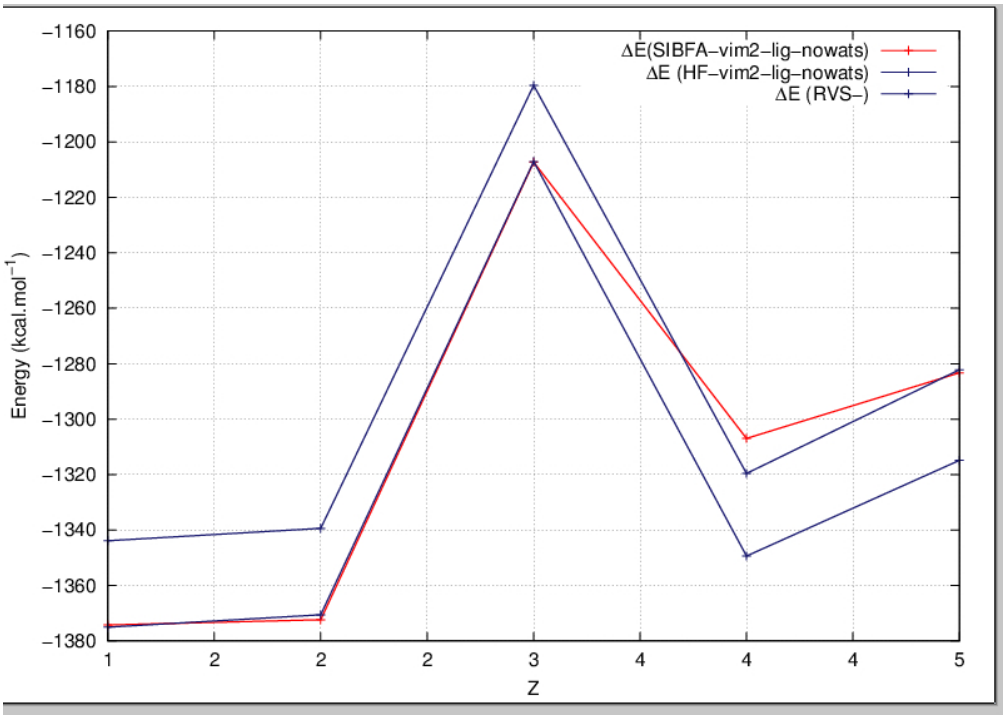
ΔE(SIBFA–vim2–lig–nowats)
ΔE (HF–vim2–lig–nowats)
ΔE (RVS–)
Energy (kcal.mol^{-1})
−1160
−1180
−1200
−1220
−1240
−1260
−1280
−1300
−1320
−1340
−1360
−1380
1
2
2
2
3
4
4
4
5
Z

Figure 3a

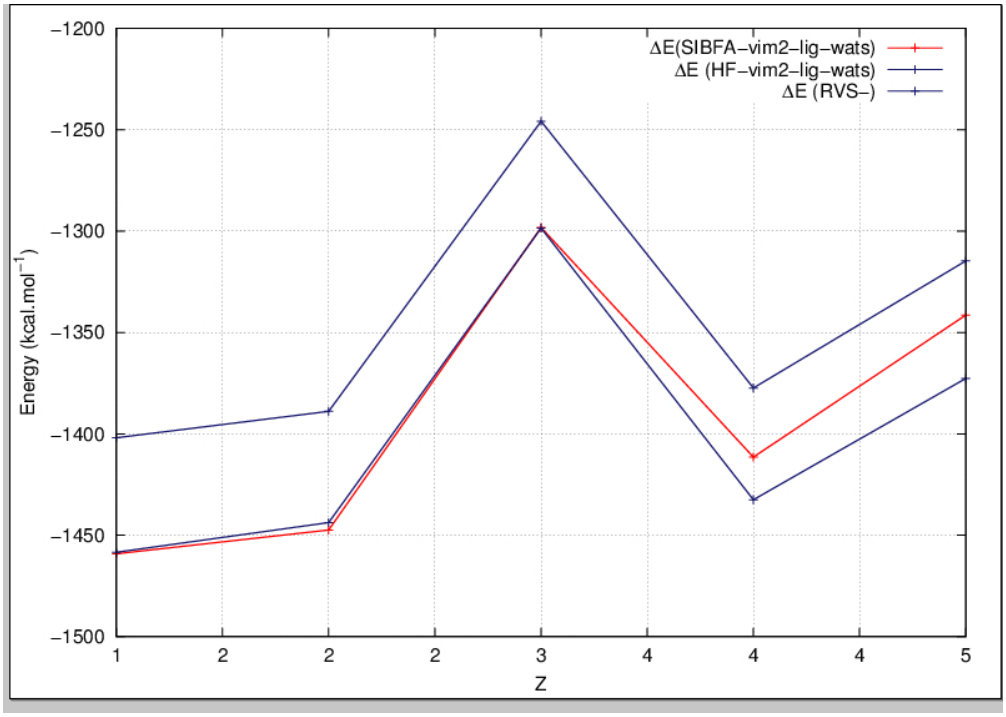
ΔE(SIBFA–vim2–lig–wats)
ΔE (HF–vim2–lig–wats)
ΔE (RVS–)
Energy (kcal.mol^{-1})
Z
−1200
−1250
−1300
−1350
−1400
−1450
−1500
1
2
2
2
3
4
4
4
5

Figure 3b

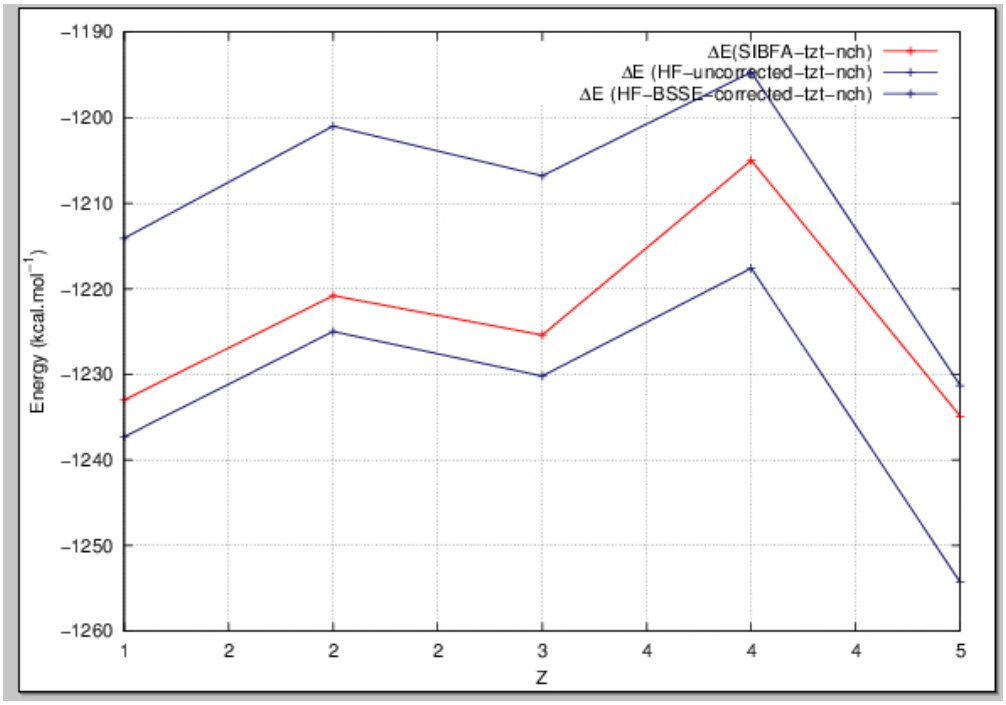
ΔE(SIBFA–tzt–nch)
ΔE (HF–uncorrected–tzt–nch)
ΔE (HF–BSSE–corrected–tzt–nch)
Energy (kcal.mol^{-1})
Z
−1190
−1200
−1210
−1220
−1230
−1240
−1250
−1260
1
2
2
2
3
4
4
4
5

Figure 3c

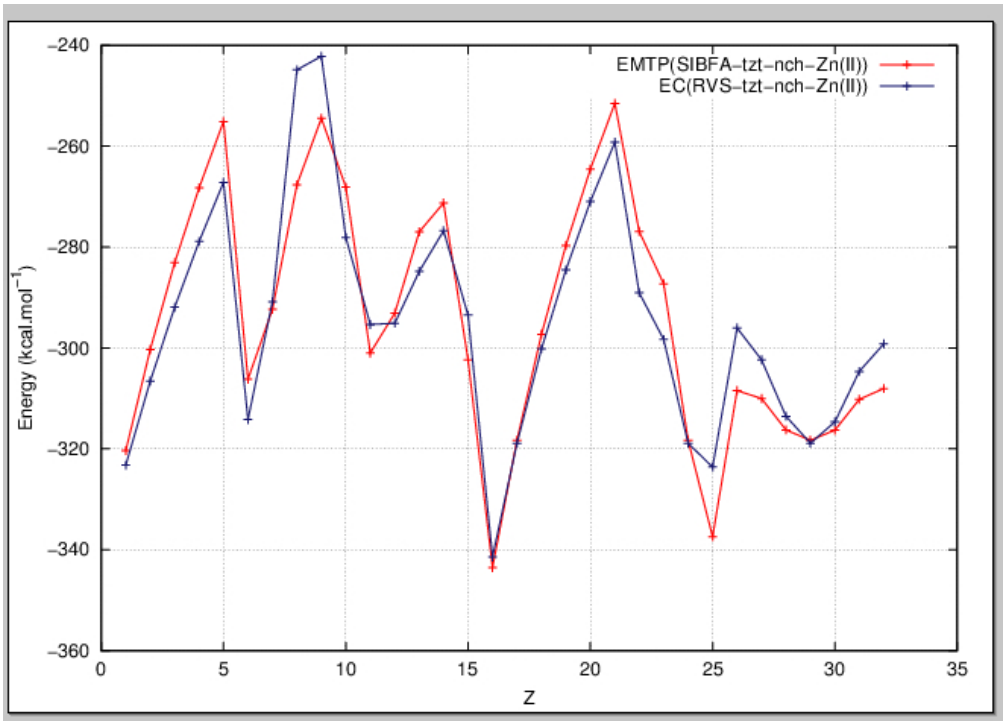
EMTP(SIBFA-tzt-nch-Zn(II))
EC(RVS-tzt-nch-Zn(II))
Energy (kcal.mol^{-1})
Z
-240
-260
-280
-300
-320
-340
-360
0
5
10
15
20
25
30
35

Figure 4 a.

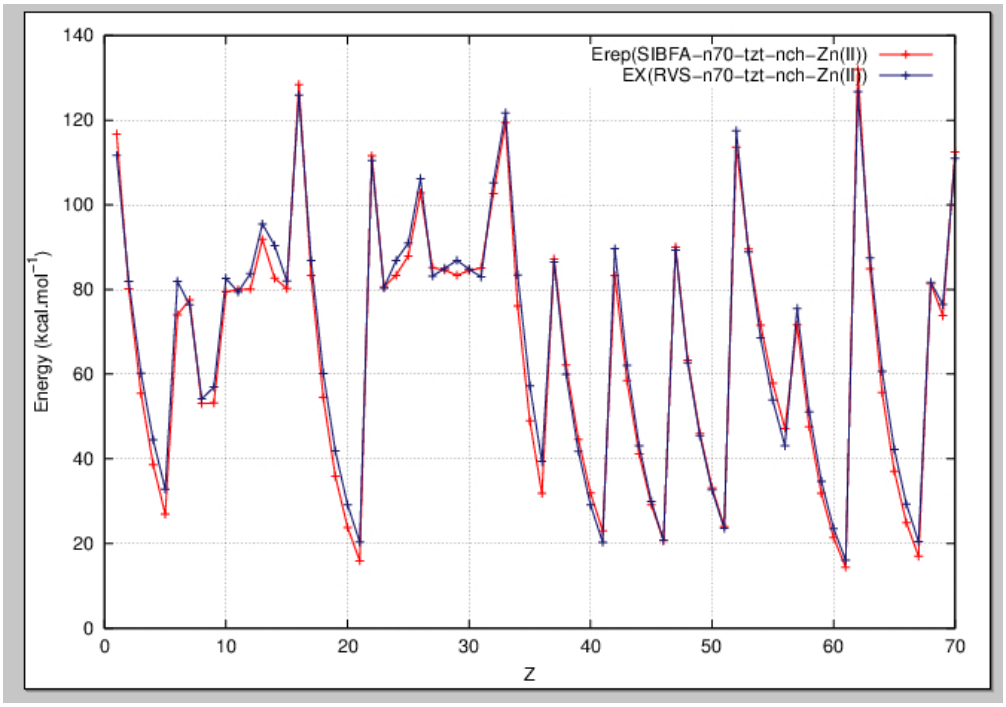
Erep(SIBFA-n70-tzt-nch-Zn(II))
EX(RVS-n70-tzt-nch-Zn(II))
Energy (kcal.mol^{-1})
Z
0
20
40
60
80
100
120
140
0
10
20
30
40
50
60
70

Figure 4b.

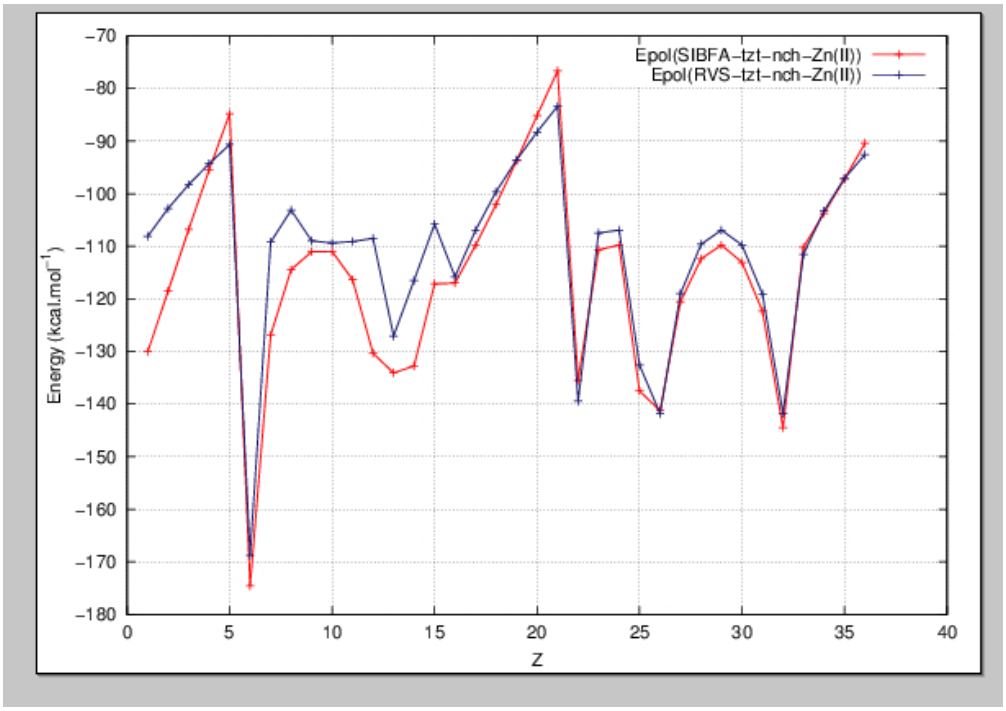
Epol(SIBFA-tzt-nch-Zn(II))
Epol(RVS-tzt-nch-Zn(II))
Energy (kcal.mol^{-1})
Z
-70
-80
-90
-100
-110
-120
-130
-140
-150
-160
-170
-180
0
5
10
15
20
25
30
35
40

Figure 4c

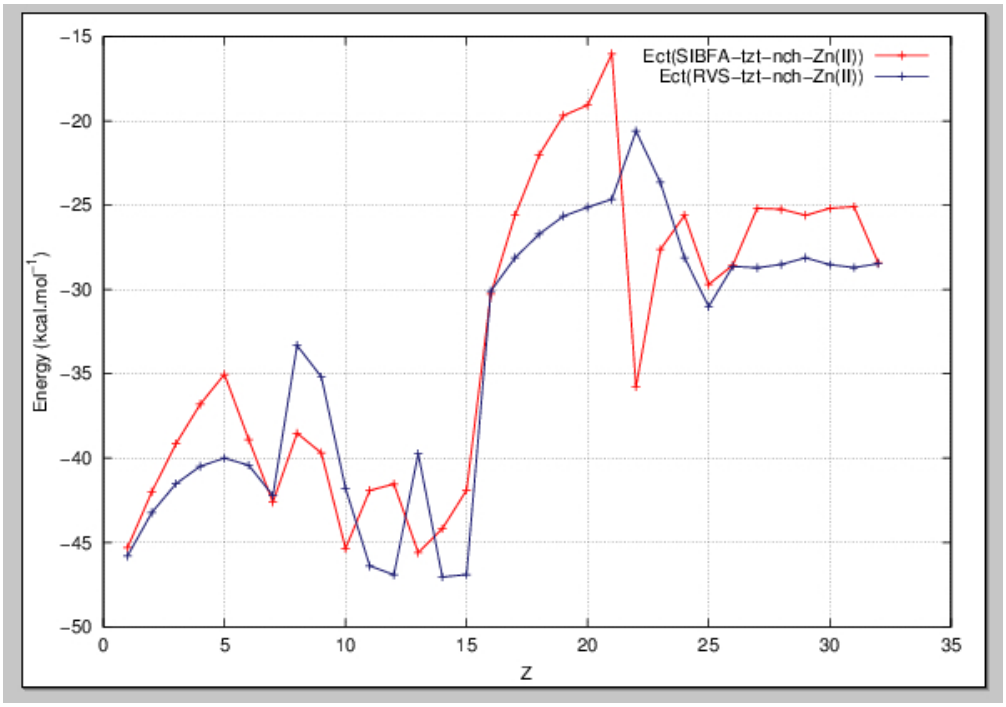
Ect(SIBFA-tzt-nch-Zn(II))
Ect(RVS-tzt-nch-Zn(II))
Energy (kcal.mol^{-1})
Z
-15
-20
-25
-30
-35
-40
-45
-50
0
5
10
15
20
25
30
35

Figure 4d

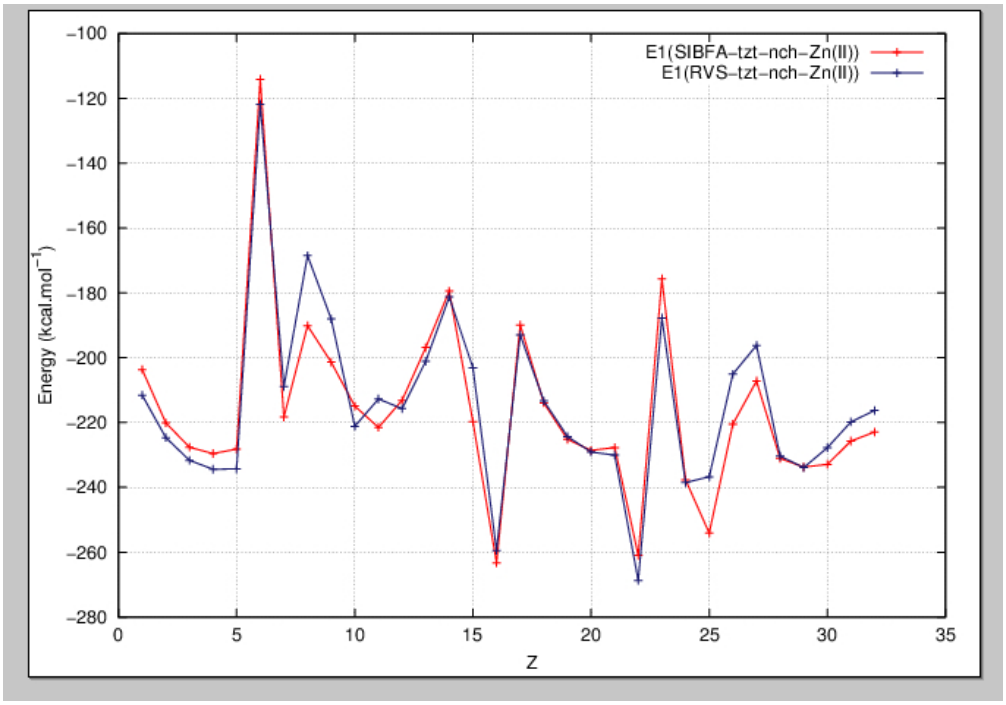
E1(SIBFA–tzt–nch–Zn(II))
E1(RVS–tzt–nch–Zn(II))
Energy (kcal.mol^{-1})
Z
−100
−120
−140
−160
−180
−200
−220
−240
−260
−280
0
5
10
15
20
25
30
35

Figure 4e.

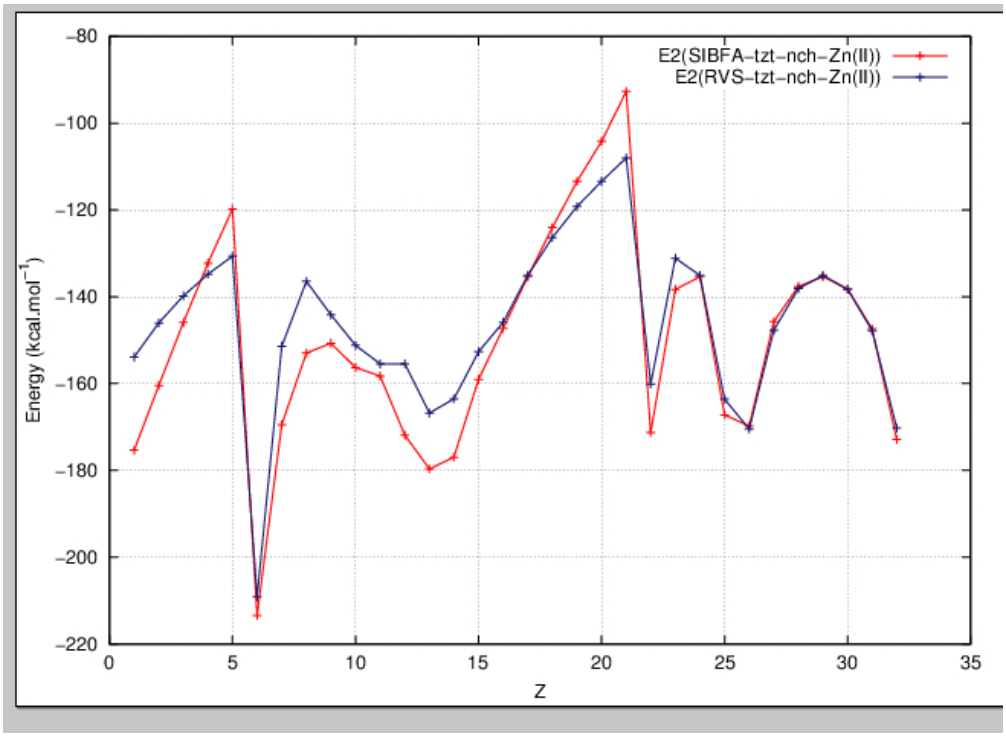
E2(SIBFA-tzt-nch-Zn(II))
E2(RVS-tzt-nch-Zn(II))
Energy (kcal.mol^{-1})
Z
-80
-100
-120
-140
-160
-180
-200
-220
0
5
10
15
20
25
30
35

Figure 4f

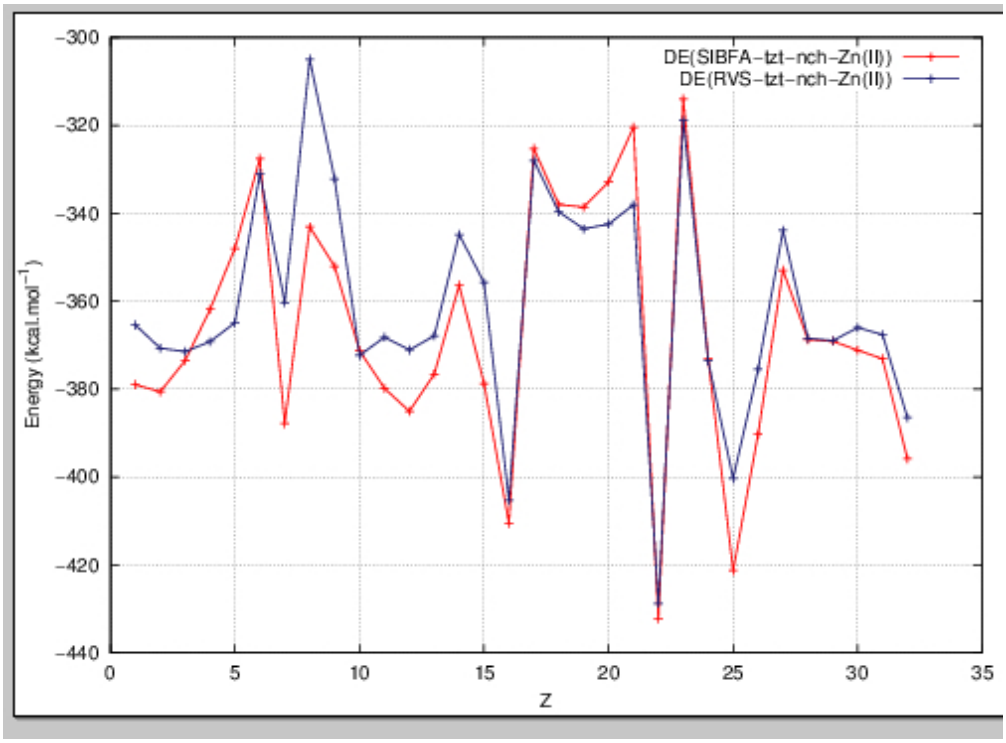
DE(SIBFA-tzt-nch-Zn(II))
DE(RVS-tzt-nch-Zn(II))
Energy (kcal.mol^{-1})
Z
-300
-320
-340
-360
-380
-400
-420
-440
0
5
10
15
20
25
30
35

Figure 4g

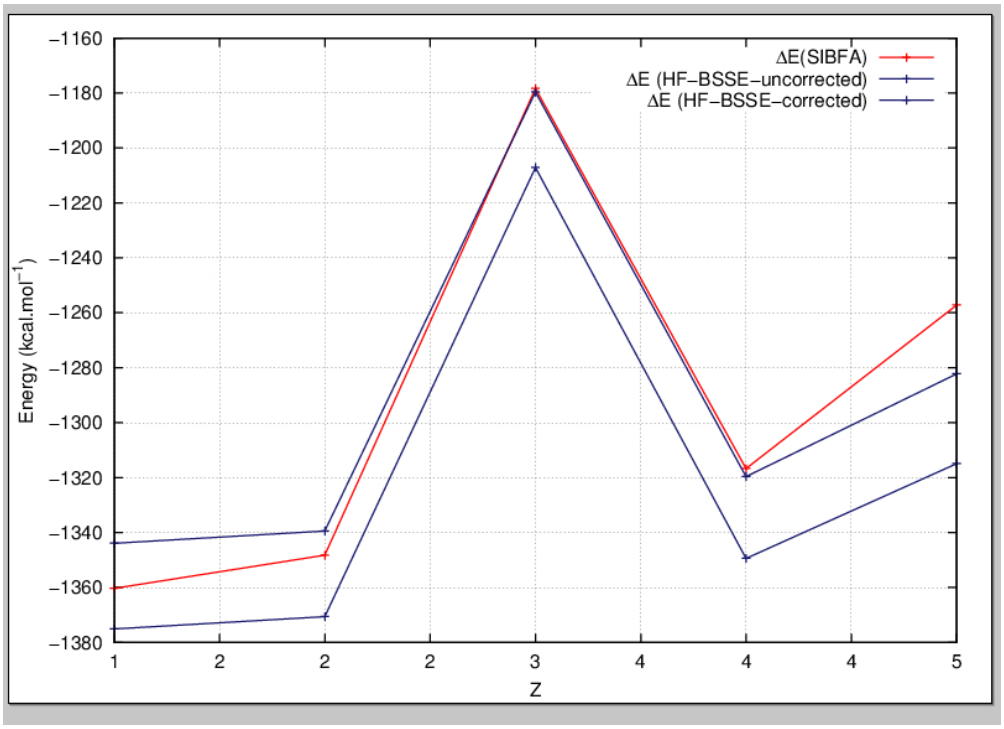
ΔE(SIBFA)
ΔE (HF–BSSE–uncorrected)
ΔE (HF–BSSE–corrected)
Energy (kcal.mol^{-1})
Z
−1160
−1180
−1200
−1220
−1240
−1260
−1280
−1300
−1320
−1340
−1360
−1380
1
2
2
2
3
4
4
4
5

Figure 5a

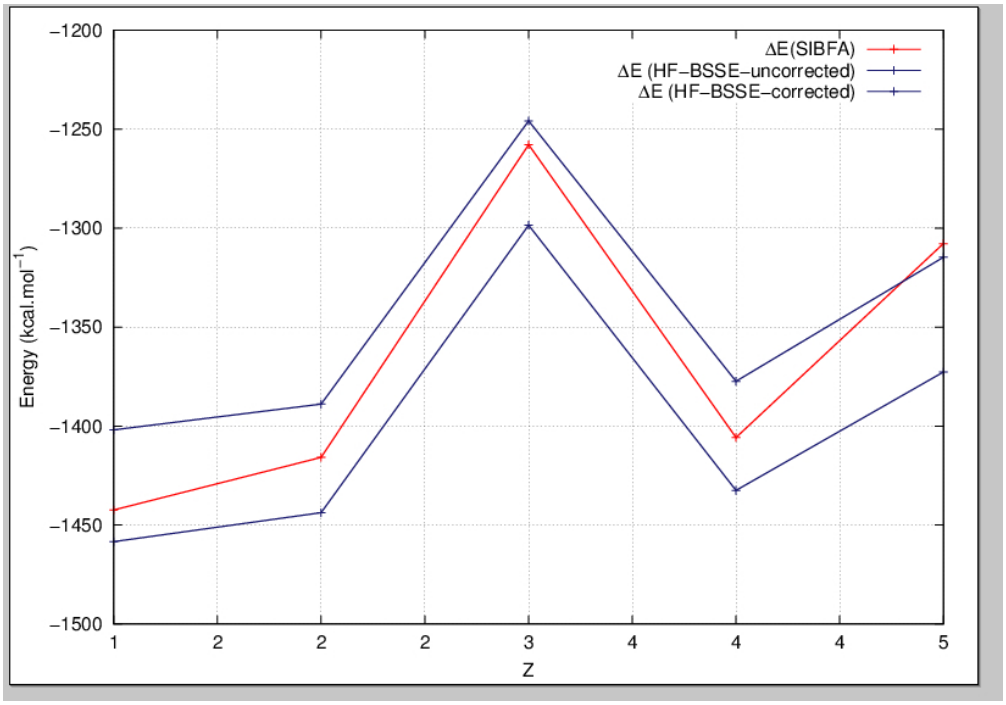
ΔE(SIBFA)
ΔE (HF–BSSE–uncorrected)
ΔE (HF–BSSE–corrected)
Energy (kcal.mol^{-1})
Z
−1200
−1250
−1300
−1350
−1400
−1450
−1500
1
2
2
2
3
4
4
4
5

Figure 5b

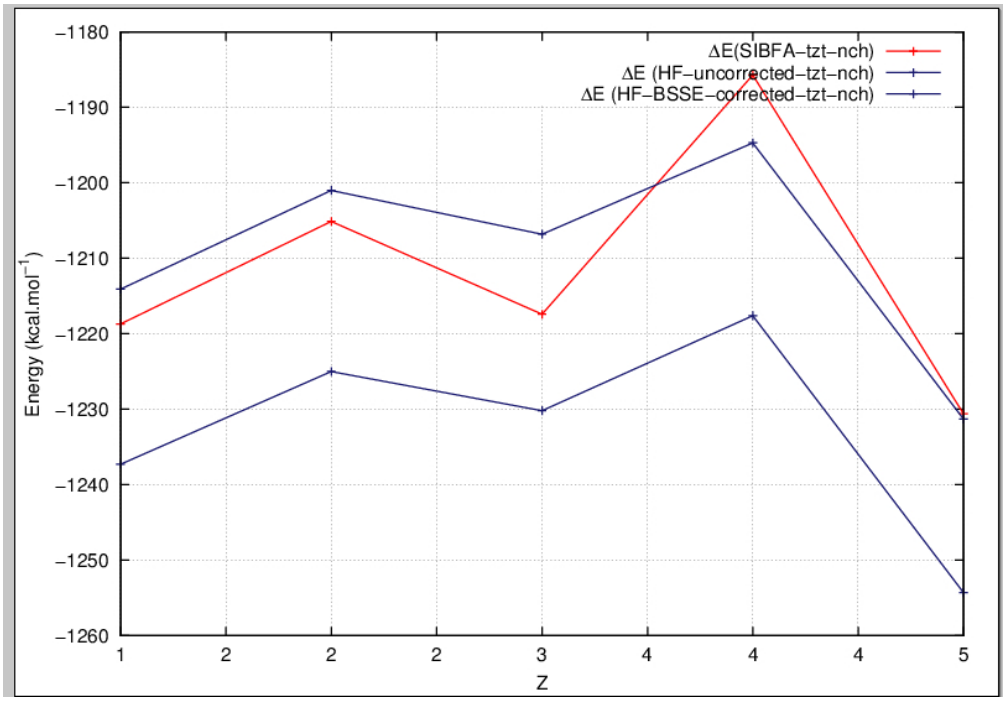
ΔE(SIBFA–tzt–nch)
ΔE (HF–uncorrected–tzt–nch)
ΔE (HF–BSSE–corrected–tzt–nch)
Energy (kcal.mol^{-1})
Z
−1180
−1190
−1200
−1210
−1220
−1230
−1240
−1250
−1260
1
2
2
2
3
4
4
4
5

Figure 5-c

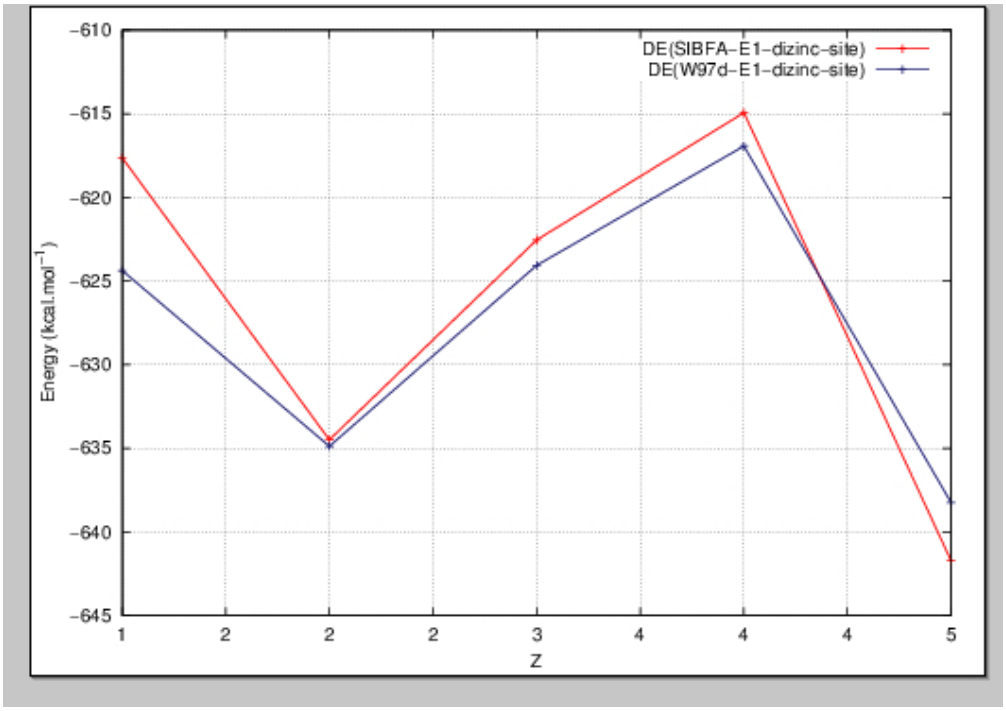
DE(SIBFA-E1-dizinc-site)
DE(W97d-E1-dizinc-site)
Energy (kcal.mol^{-1})
Z
-610
-615
-620
-625
-630
-635
-640
-645
1
2
2
2
3
4
4
4
5

Figure 6-a

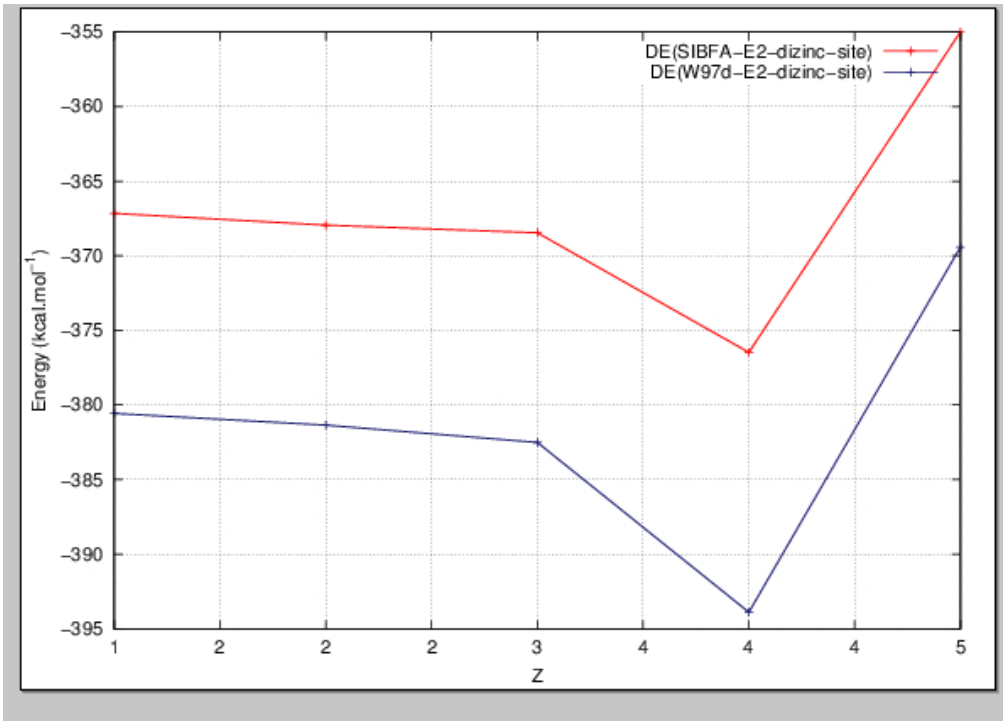
DE(SIBFA–E2–dizinc–site)
DE(W97d–E2–dizinc–site)
Energy (kcal.mol^{-1})
Z
−355
−360
−365
−370
−375
−380
−385
−390
−395
1
2
2
2
3
4
4
4
5

Figure 6-b

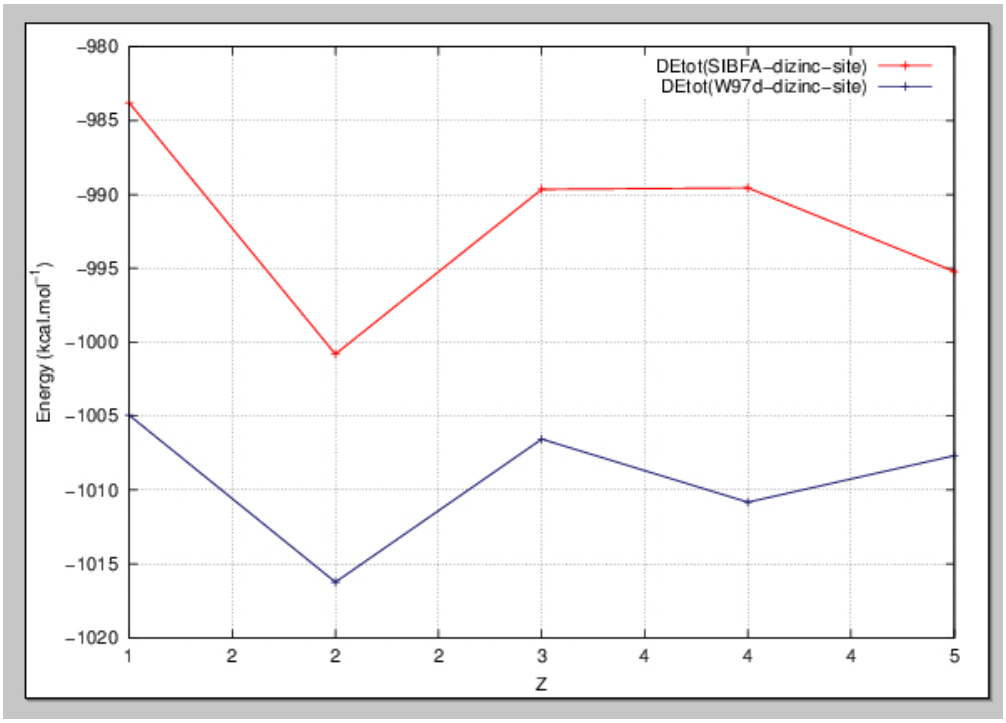
DEtot(SIBFA–dizinc–site)
DEtot(W97d–dizinc–site)
Energy (kcal.mol^{-1})
Z
–980
–985
–990
–995
–1000
–1005
–1010
–1015
–1020
1
2
2
2
3
4
4
4
5

Figure 6-c

Table I. Complexes of the extended recognition site of VIM-2 with ligands I-V. Compared ΔE(SIBFA) and ΔE(QC/HF) on the following:

a) intermolecular interactions prior to ligand binding and without the 'discrete' water molecules; b) intermolecular interactions prior to ligand binding and with the 'discrete' water molecules; c) intermolecular interactions with the TZT anchor and without the waters; d) intermolecular interactions with the entire ligands and without the waters; e) intermolecular interactions with the entire ligands and with the waters. Energies in kcal/mol. The ΔE(QC) BSSE-corrected values are given in bold. Energies in kcal/mol.

	a) Nolig-nowats		b) Nolig		c) Tzt		d) Lig-nowats		e) Lig-wats	
	SIBFA	QC	SIBFA	QC	SIBFA	QC	SIBFA	QC	SIBFA	QC
Lig-4690	**-997.9**	1013.5/ **-995.9**	**-1076.7**	-1095.1/ **-1055.3**	**-1233.0**	-1237.3/ **-1214.1**	**-1374.3**	-1375.2/ **-1343.9**	**-1459.2**	-1458.4/ **-1401.9**
Lig-4390	**-1000.2**	-1011.6/ **-993.1**	**-1066.5**	-1081.8/ **-1041.4**	**-1220.8**	-1225.0/ **-1201.0**	**-1372.4**	-1370.6/ **-1339.4**	**-1447.4**	-1443.8/ **-1388.9**
Lig-4684	**-990.5**	-1008.8/ **-991.1**	**-1085.8**	-1108.7/ **-1068.6**	**-1225.4**	-1230.2/ **-1206.8**	**-1207.3**	-1207.1/ **-1179.6**	**-1298.2**	-1298.5/ **-1245.8**
Lig-5064	**-993.0**	-1004.2/ **-986.6**	**-1069.3**	-1085.9/ **-1045.3**	**-1205.0**	-1217.6/ **-1194.7**	**-1307.0**	-1349.4/ **-1319.6**	**-1411.5**	-1432.5/ **-1377.4**
Lig-5069	**-996.3**	-1022.6/ **-1004.8**	**-1055.6**	-1085.2/ **-1044.3**	**-1234.9**	-1254.3/ **-1231.3**	**-1283.3**	-1314.9/ **-1282.9**	**-1341.4**	-1372.7/ **-1314.7**

Table II. Mono-zinc binding sites of VIM-2 in their complexes with the five inhibitors. QC (HF/RVS) and SIBFA intermolecular interaction energies and their contributions. Energies in kcal/mol.

Blue core unbound										
	I. Lig-4690		II. Lig-4390		III. Lig-4684		IV. Lig-5064		V. Lig-5069	
	QC	SIBFA	QC	SIBFA	QC	SIBFA`	QC	SIBFA	QC	SIBFA
EC/EMTP	-271.6	-278.4	-290.2	-297.5	-284.8	-292.6	-304.1	-311.8	-275.5	-282.3
EX/Erep	118.0	125.5	145.6	153.0	138.0	145.8	166.5	173.0	131.8	139.2
E1	**-153.5**	**-152.9**	**-144.6**	**-144.6**	**-146.8**	**-146.8**	**-137.5**	**-138.8**	**-143.9**	**-143.1**
Epol	-125.2	-123.9	-130.3	-126.4	-129.9	-126.8	-137.8	-130.4	-126.3	-123.0
Ect	-33.4	-30.7	-35.3	-33.5	-35.0	-32.9	-37.6	-34.2	-33.8	-32.1
E2	**-158.6**	**-154.7**	**-165.7**	**-159.9**	**-164.9**	**-159.7**	**-175.4**	**-164.5**	**-160.1**	**-155.1**
ΔE	**-312.1**	**-308.2**	**-310.3**	**-305.3**	**-311.7**	**-307.3**	**-313.0**	**-305.4**	**-303.9**	**-299.7**

Colored core unbound										
	I. Lig-4690		II. Lig-4390		III. Lig-4684		IV. Lig-5064		V. Lig-5069	
	QC	SIBFA	QC	SIBFA	QC	SIBFA`	QC	SIBFA	QC	SIBFA
EC/EMTP	-559.9	-549.6	-568.6	-561.6	-553.8	-545.3	-563.3	-556.0	-568.6	-559.5
EX/Erep	99.8	88.0	107.7	95.9	94.9	84.2	104.6	93.2	116.4	107.5
E1	**-458.1**	**-461.6**	**-460.9**	**-465.6**	**-459.0**	**-461.2**	**-458.7**	**-462.8**	**-452.3**	**-452.0**
Epol	-89.7	-94.5	-92.3	-96.0	-89.9	-99.3	-91.1	-95.5	-96.1	-99.0
Ect	-40.0	-34.8	-40.5	-35.6	-39.0	-34.2	-40.2	-35.5	-40.1	-35.0
E2	**-129.8**	**-129.3**	**-132.8**	**-131.6**	**-128.9**	**-130.0**	**-131.3**	**-131.0**	**-136.2**	**-134.0**
ΔE	**-587.9**	**-594.8**	**-594.7**	**-600.8**	**-587.9**	**-594.8**	**-590.0**	**-598.1**	**-588.5**	**-588.9**

Blue core bound										
	I. Lig-4690		II. Lig-4390		III. Lig-4684		IV. Lig-5064		V. Lig-5069	
	QC	SIBFA	QC	SIBFA	QC	SIBFA`	QC	SIBFA	QC	SIBFA
EC/EMTP	-547.3	-555.7	-557.2	-562.9	-566.0	-574.9	-579.3	-583.4	-532.3	-533.9
EX/Erep	198.3	200.5	214.3	217.5	227.8	230.6	256.2	260.8	189.8	193.4
E1	**-349.3**	**-355.3**	**-342.9**	**-345.4**	**-338.2**	**-344.3**	**-323.0**	**-322.6**	**-342.4**	**-340.4**
Epol	-131.1	-130.6	-133.9	-130.5	-135.4	-131.9	-141.2	-133.7	-128.7	-128.4
Ect	-37.7	-31.6	-39.5	-33.4	-40.6	-33.7	-43.2	-35.3	-38.9	-32.1
E2	**-168.9**	**-162.2**	**-173.4**	**-163.9**	**-176.0**	**-165.5**	**-184.3**	**-169.0**	**-167.5**	**-160.5**
ΔE	**-518.1**	**-520.6**	**-516.3**	**-511.7**	**-514.2**	**-513.2**	**-507.4**	**-492.7**	**-510.0**	**-503.3**

Colored core bound										
	I. Lig-4690		II. Lig-4390		III. Lig-4684		IV. Lig-5064		V. Lig-5069	
	QC	SIBFA	QC	SIBFA	QC	SIBFA`	QC	SIBFA	QC	SIBFA
EC/EMTP	-690.4	-704.5	-693.9	-709.8	-683.9	-699.9	-687.5	-700.8	-655.6	-658.1
EX/Erep	231.3	232.4	240.0	244.2	226.5	224.5	226.2	227.0	179.0	171.8
E1	**-459.2**	**-472.2**	**-453.9**	**-465.5**	**-457.4**	**-475.4**	**-461.3**	**-473.8**	**-476.6**	**-486.2**
Epol	-99.3	-96.4	-101.6	-97.0	-99.1	-99.3	-98.9	-94.3	-94.6	-93.6
Ect	-48.4	-43.0	-48.0	-42.8	-47.9	-42.3	-47.5	-42.4	-43.6	-38.0
E2	**-147.7**	**-139.4**	**-149.7**	**-139.7**	**-147.0**	**-141.6**	**-146.4**	**-136.7**	**-138.2**	**-131.7**
ΔE	**-606.8**	**-613.3**	**-603.5**	**-606.1**	**-604.4**	**-618.3**	**-607.7**	**-612.3**	**-614.7**	**-618.8**

Table III. Di-zinc cores of Vim-2 in their complexes with the five inhibitors. QC (HF/RVS) and SIBFA intermolecular interaction energies. Energies in kcal/mol. **(**a) and (b): QC results with the ccp-pVTZ and augcc-pVTZ basis sets, respectively.

Dizinc core unbound										
	I. Lig-4690		II. Lig-4390		III. Lig-4684		IV. Lig-5064		V. Lig-5069	
	QC	SIBFA	QC	SIBFA	QC	SIBFA`	QC	SIBFA	QC	SIBFA
ΔE (a)	-915.6	-912.7	-914.9	-921.8	-916.6	-913.7	-919.2	-914.7	-921.4	-908.1
ΔE (b)	**-914.0**	**-912.7**	**-921.6**	**-921.8**	**-912.3**	**-913.7**	**-914.8**	**-914.7**	**-917.2**	**-908.1**

Dizinc core bound										
	I. Lig-4690		II. Lig-4390		III. Lig-4684		IV. Lig-5064		V. Lig-5069	
	QC	SIBFA	QC	SIBFA	QC	SIBFA	QC	SIBFA	QC	SIBFA
ΔE (a)	-1116.8	-1113.1	-1117.0	-1109.0	-1113.6	-1118.5	-1111.3	-1096.7	-1131.0	-1124.3
ΔE (b)	**-1116.8**	**-1113.1**	**-1117.7**	**-1109.0**	**-1111.2**	**-1118.5**	**-1109.5**	**-1096.7**	**-1128.5**	**-1124.3**

Table IV. Complexes of the extended recognition site of VIM-2 with ligands I-V. Compared ΔE(SIBFA) and ΔE(QC/HF) at the outcome of the recalibration procedure on the following:

a) intermolecular interactions prior to ligand binding and without the 'discrete' water molecules; b) intermolecular interactions prior to ligand binding and with the 'discrete' water molecules; c) intermolecular interactions with the TZT anchor and without the waters; d) intermolecular interactions with the entire ligands and without the waters; e) intermolecular interactions with the entire ligands and with the waters. The BSSE-corrected ΔE(QC) values are given in bold. Energies in kcal/mol.

	a) Nolig-nowats		b) Nolig		c) Tzt-nch		d) Lig-nowats		e) Lig-wats	
	SIBFA	QC	SIBFA	QC	SIBFA	QC	SIBFA	QC	SIBFA	QC
Lig-4690	**-1002.4**	1013.5/ **-995.9**	**-1073.4**	-1095.1/ **-1055.3**	**-1217.1**	-1237.3/ **-1214.1**	**-1346.1**	-1375.2/ **-1343.9**	**-1426.1**	-1458.4/ **-1401.9**
Lig-4390	**-1001.4**	-1011.6/ **-993.1**	**-1060.2**	-1081.8/ **-1041.4**	**-1204.8**	-1225.0/ **-1201.0**	**-1336.9**	-1370.6/ **-1339.4**	**-1405.5**	-1443.8/ **-1388.9**
Lig-4684	**-992.4**	-1008.8/ **-991.1**	**-1080.5**	-1108.7/ **-1068.6**	**-1217.1**	-1230.2/ **-1206.8**	**-1182.0**	-1207.1/ **-1179.6**	**-1261.3**	-1298.5/ **-1245.8**
Lig-5064	**-985.4**	-1004.2/ **-986.6**	**-1060.4**	-1085.9/ **-1045.3**	**-1188.3**	-1217.6/ **-1194.7**	**-1303.9**	-1349.4/ **-1319.6**	**-1391.9**	-1432.5/ **-1377.4**
Lig-5069	**-995.4**	-1022.6/ **-1004.8**	**-1045.0**	-1085.2/ **-1044.3**	**-1231.4**	-1254.3/ **-1231.3**	**-1270.7**	-1314.9/ **-1282.9**	**-1328.4**	-1372.7/ **-1314.7**

Table Va.

Lig-4690. Compared ΔE(RVS) and ΔE(SIBFA) values for the binding of the R2 benzocarboxylate arm with the Tyr67, Arg228, and His263 side-chains.

	Benzocarboxylate-Tyr67		Benzocarboxylate-Arg228		Benzocarboxylate-His263	
	RVS	SIBFA	RVS	SIBFA	RVS	SIBFA
E_C/E_{MTP}	1.4	1.7	-57.5	-56.4	-0.8	-4.2
E_{exch}/E_{rep}	1.9	2.0	4.7	4.6	13.6	12.0
E_1	3.2	3.7	-52.8	-51.9	12.8	8.2
E_{pol}	-0.7	-0.7	-4.1	-3.4	-2.7	-2.0
E_{ct}	0.0	0.0	-0.1	-0.2	-0.4	-0.1
E_2	-0.7	-0.7	-4.2	-3.9	-3.1	-2.1
ΔE	**2.5**	**3.0**	**-57.0**	**-55.5**	**10.5**	**5.6**

Lig-4690. Compared ΔE(RVS) and ΔE(SIBFA) values for the binding of the R2 benzocarboxylate arm with the main-chain of Asn233.

	Asn233	
	RVS	SIBFA
E_C/E_{MTP}	-24.1	-30.3
E_{exch}/E_{rep}	15.7	14.3
E_1	-8.5	-13.8
E_{pol}	-7.7	-6.3
E_{ct}	-1.7	-1.9
E_2	-9.4	-8.2
ΔE	**-17.9**	**-24.8**

Lig-4690. Compared ΔE(RVS) and ΔE(SIBFA) values for the binding of the R1 arm with the Phe61 and Trp87 side-chains.

	o-methoxy—Phe61		o-methoxy—Trp87	
	RVS	SIBFA	RVS	SIBFA
E_C/E_{MTP}	-2.7	-5.1	-3.9	-5.0
E_{exch}/E_{rep}	6.1	6.7	7.6	6.7
E_1	3.3	1.5	3.8	2.9
E_{pol}	-0.8	-0.2	-1.4	-0.7
E_{ct}	-0.2	-0.1	-0.2	-0.4
E_2	-1.0	-0.3	-1.6	-1.1
ΔE	**2.3**	**1.3**	**2.2**	**1.3**

Table Vb.

Lig-4390. Compared ΔE(RVS) and ΔE(SIBFA) values for the binding of the R2 benzocarboxylate side-chain with the Arg228 and His263 side-chains.

	Benzocarboxylate-Arg228		Benzocarboxylate-His263	
	RVS	SIBFA	RVS	SIBFA
E_C/E_{MTP}	-55.9	-55.0	2.5	0.0
E_{exch}/E_{rep}	4.2	4.3	5.5	5.9
E_1	-51.7	-50.7	8.0	5.9
E_{pol}	-3.7	-3.1	-2.7	-1.7
E_{ct}	-0.1	-0.2	-0.1	-0.1
E_2	-3.8	-3.3	-2.8	-1.8
ΔE	**-55.5**	**-54.0**	**5.2**	**4.1**

Lig-4390. Compared ΔE(RVS) and ΔE(SIBFA) values for the binding of the R2 benzocarboxylate arm with the main-chain of Asn233.

	Asn233	
	RVS	SIBFA
E_C/E_{MTP}	-28.2	-36.6
E_{exch}/E_{rep}	22.7	24.9
E_1	-5.5	-11.7
E_{pol}	-9.7	-7.3
E_{ct}	-3.3	-3.0
E_2	-13.0	-10.4
ΔE	**-18.5**	**-22.1**

Lig-4390. Compared ΔE(RVS) and ΔE(SIBFA) values for the binding of the R1 benzene side-chain with the Phe61 and Trp87 side-chains.

	Benzene-Phe61		Benzene-Trp87	
	RVS	SIBFA	RVS	SIBFA
E_C/E_{MTP}	-1.4	-3.1	-1.4	-2.8
E_{exch}/E_{rep}	2.9	3.7	4.8	4.5
E_1	1.5	0.6	3.4	1.7
E_{pol}	-0.5	-0.1	-0.8	-0.4
E_{ct}	-0.0	-0.0	-0.2	-0.2
E_2	-0.5	-0.1	-1.0	-0.6
ΔE	**1.1**	**0.4**	**2.4**	**1.1**

Table Vc.

Lig-4684. Compared ΔE(RVS) and ΔE(SIBFA) values for the binding of the R2 N-hydrazone-connected dihydroxy-phenyl arm with the Arg228, and His263 and Tyr67 side-chains.

	Dihydroxy-phenyl-Arg228		Dihydroxy-phenyl-His263		Dihydroxy-phenyl-Tyr67	
	RVS	RVS	RVS	SIBFA	RVS	SIBFA
E_C/E_{MTP}	-7.2	-7.5	-2.3	-4.5	-3.1	-4.2
E_{exch}/E_{rep}	3.6	4.3	5.6	8.3	8.3	8.4
E_1	-3.6	-3.2	3.3	3.7	5.2	4.2
E_{pol}	-3.8	-2.5	-0.7	-0.4	-1.3	-0.6
E_{ct}	-0.2	-0.1	-0.1	-0.2	-0.5	-0.4
E_2	-4.0	-2.7	-0.8	-0.6	-1.8	-1.0
ΔE	**-7.6**	**-5.9**	**2.5**	**3.2**	**3.4**	**3.2**

Lig-4684. Compared ΔE(RVS) and ΔE(SIBFA) values for the binding of the R1 dihydroxy-phenyl arm with the Phe61 and Trp87 side-chains.

	Dihydroxy-phenyl-Phe61		Dihdyroxy-phenyl-Trp87	
	RVS	SIBFA	RVS	SIBFA
E_C/E_{MTP}	-1.3	-3.2	-9.3	-8.9
E_{exch}/E_{rep}	3.2	3.8	15.8	15.8
E_1	1.9	0.6	6.5	6.9
E_{pol}	-0.5	-0.1	-2.4	-0.9
E_{ct}	-0.1	-0.1	-1.1	-1.4
E_2	-0.6	-0.2	-3.5	-2.3
ΔE	**1.3**	**0.4**	**3.0**	**4.6**

Table Vd.

Lig-5064. Compared ΔE(RVS) and ΔE(SIBFA) values for the binding of the R2 benzocarboxylate arm with the Arg228 and His263 side-chains.

	Benzocarboxylate-Arg228		Benzocarboxylate-His263	
	RVS	RVS	RVS	SIBFA
E_C/E_{MTP}	-55.1	-53.4	3.9	2.4
E_{exch}/E_{rep}	3.2	3.4	1.9	2.7
E_1	-51.9	-50.0	5.8	5.1
E_{pol}	-3.3	-3.1	-1.3	-1.5
E_{ct}	-0.2	-0.1	0.0	-0.1
E_2	-3.5	-3.2	-1.3	-1.6
ΔE	**-55.5**	**-53.2**	**4.5**	**3.5**

Lig-5064. Compared ΔE(RVS) and ΔE(SIBFA) values for the binding of the R2 benzocarboxylate arm with the central backbone of Arg228.

	Benzocarboxylate-Arg228	
	RVS	SIBFA
E_C/E_{MTP}	-31.1	-41.9
E_{exch}/E_{rep}	30.4	32.7
E_1	-0.7	-9.3
E_{pol}	-11.7	-8.3
E_{ct}	-4.8	-3.5
E_2	-16.5	-11.8
ΔE	**-17.2**	**-21.0**

Lig-5064. Compared ΔE(RVS) and ΔE(SIBFA) values for the binding of the R1 dichlorophenyl arm with the Phe61, Trp87, and Asp119 side-chains.

	Dichlorophenyl-Phe61		Dichlorophenyl-Trp87		Dichlorophenyl-Asp119	
	RVS	SIBFA	RVS	SIBFA	RVS	SIBFA
E_C/E_{MTP}	-6.6	-11.8	-3.1	-3.6	-2.6	-6.7
E_{exch}/E_{rep}	17.9	19.2	7.9	11.7	9.9	12.0
E_1	11.3	8.0	4.9	8.1	7.3	5.3
E_{pol}	-0.9	-0.2	-1.1	-0.5	-5.2	-5.5
E_{ct}	-0.8	-0.0	-0.3	-0.4	-0.7	-0.0
E_2	-1.7	-0.2	-1.4	-0.9	-5.9	-5.5
ΔE	**9.6**	**7.8**	**3.5**	**7.3**	**1.4**	**-0.2**

Table Ve.

Lig-5069. Compared ΔE(RVS) and ΔE(SIBFA) values for the binding of the N-hydrazone substituting benzene of arm R2 with Tyr 67 and Arg228 side-chains.

	Benzene-Tyr67		Benzene-Arg228	
	RVS	RVS	RVS	SIBFA
E_C/E_{MTP}	-3.6	-5.2	-1.9	-3.4
E_{exch}/E_{rep}	10.1	13.4	3.0	2.9
E_1	6.5	8.2	1.1	-0.5
E_{pol}	-1.0	-0.4	-3.5	-2.1
E_{ct}	-0.4	-0.1	-0.3	-0.1
E_2	-1.4	-0.5	-3.3	-2.2
ΔE	**5.1**	**7.7**	**-2.2**	**-2.7**

Lig-5069. Compared ΔE(RVS) and ΔE(SIBFA) values for the binding of the benzocarboxylate of the R2 arm with the Arg228 and His263 side-chains.

	Benzocarboxylate-Arg228		Benzocarboxylate-His263	
	RVS	SIBFA	RVS	SIBFA
E_C/E_{MTP}	-62.1	-59.0	-24.0	-28.0
E_{exch}/E_{rep}	14.4	15.4	54.3	47.7
E_1	-47.7	-43.6	30.2	19.7
E_{pol}	-8.8	-6.8	-8.1	-6.3
E_{ct}	-2.1	-1.0	-3.5	-2.1
E_2	-10.9	-7.8	-11.6	-8.4
ΔE	**-58.6**	**-51.4**	**18.6**	**11.4**

Lig-5069. Compared ΔE(RVS) and ΔE(SIBFA) values for the binding of the benzocarboxylate of the R2 arm with the Glu225 main-chain.

	Benzocarboxylate-Glu225 backbone	
	RVS	SIBFA
E_C/E_{MTP}	-7.8	-10.9
E_{exch}/E_{rep}	0.7	1.7
E_1	-7.1	-9.2
E_{pol}	-2.2	-1.9
E_{ct}	-0.0	-0.4
E_2	-2.2	-2.3
ΔE	**-9.3**	**-11.5**

Lig-5069. Compared ΔE(RVS) and ΔE(SIBFA) values for the binding of the R1 dihydroxyphenyl group with the Trp87 side-chain.

	Dihydroxyphenyl-Trp87	
	RVS	SIBFA
E_C/E_{MTP}	-5.7	-6.1
E_{exch}/E_{rep}	6.8	6.9
E_1	1.1	0.8
E_{pol}	-1.4	-0.7
E_{ct}	-0.4	-0.7
E_2	-1.8	-1.4
ΔE	**-0.7**	**-0.7**

Table VI. Mono-zinc binding sites of Vim-2 in their complexes with the five inhibitors. ALMOEDA DFT, HF, and SIBFA intermolecular interaction energies and their contributions. Energies in kcal/mol.

Blue core unbound					
	I. Lig-4690	II. Lig-4390	III. Lig-4684	IV. Lig-5064	V. Lig-5069
E1(B3LYP)	**-159.8**	**-152.5**	**-154.5**	**-146.2**	**-151.2**
E1(ωB97X-D)	**-166.6**	**-159.7**	**-161.6**	**-153.0**	**-157.7**
E1(SIBFA)	**-167.7**	**-161.1**	**-163.6**	**-156.4**	**-158.6**
E1(HF)	-158.1	-149.7	-151.9	-142.6	-148.6
Epol(B3LYP)	-138.5	-144.1	-143.7	-151.9	-138.9
Ect(B3LYP)	-52.5	-53.4	-53.1	-55.7	-53.9
E2(B3LYP)	**-192.0**	**-177.5**	**-196.8**	**-207.7**	**-192.8**
Epol**(ωB97X-D)**	-137.8	-143.5	-143.1	-151.6	-138.1
Ect**(ωB97X-D)**	-48.9	-50.2	-49.8	-52.7	-50.4
E2(ωB97X-D)	**-186.6**	**-193.7**	**-192.8**	**-204.3**	**-188.5**
Epol(SIBFA)	-127.8	-128.1	-130.0	-131.7	-128.5
Ect(SIBFA)	-28.8	-31.2	-30.3	-32.7	-29.6
E2(SIBFA)	-154.5	-159.2	-160.3	-164.4	-156.9
Edisp(SIBFA)	-18.3	-21.1	-20.2	-23.2	-19.2
E2+Edisp	**-172.9**	**-180.3**	**-180.5**	**-187.6**	**-176.0**
Epol(HF)	-123.5	-128.5	-128.1	-136.0	-123.7
Ect(HF)	-32.4	-34.1	-33.7	-36.5	-33.5

E2(HF)	-155.9	-162.6	-161.8	-172.5	-157.2
ΔE(B3LYP)	**-350.8**	**-350.0**	**-351.3**	**-353.9**	**-344.0**
ΔE(ωB97X-D)	**-353.2**	**-353.4**	**-354/4**	**-357.3**	**-346.1**
ΔEtot(SIBFA)	**-341.8**	**-340.1**	**-342.9**	**-342.4**	**-334.8**
ΔE(HF)	-314.0	**-312.3**	**-313.7**	**-315.1**	**-305.8**

Colored core unbound					
	I. Lig-4690	II. Lig-4390	III. Lig-4684	IV. Lig-5064	V. Lig-5069
E1(B3LYP)	**-471.8**	**-475.5**	**-472.0**	**-472.6**	**-466.3**
E1(ωB97X-D)	**-472.8**	**-476.6**	**-473.2**	**-473.7**	**-467.4**
E1(SIBFA)	**-469.2**	**-478.4**	**-472.2**	**-471.0**	**-473.9**
E1(HF)	-471.1	-473.7	-470.7	-470.9	-464.2
Epol(B3LYP)	-93.6	-97.7	-94.6	-96.0	-102.7
Ect(B3LYP)	-67.3	-65.3	-66.3	-66.6	-63.9
E2(B3 LYP)	**-160.9**	**-163.0**	**-160.9**	**-162.6**	**-166.6**
Epol(W97-D)	-93.1	-97.6	-94.3	-95.8	-102.6
Ect(W97-D)	-62.5	-61.2	-61.4	-62.0	-59.8
E2(ωB97X-D)	**-155.6**	**-158.7**	**-155.7**	**-157.8**	**-162.4**
Epol(SIBFA)	-104.2	-105.5	-105.2	-102.3	-102.6
Ect(SIBFA)	-32.2	-33.0	-31.6	-33.0	-33.2
E2(SIBFA)	-136.4	-136.7	-136.8	-138.0	-140.0
Edisp(SIBFA)	-14.0	-14.9	-13.4	-14.3	-16.0
E2+Edisp	**-150.4**	**-151.5**	**-150.2**	**-152.3**	**-156.0**
Epol(HF)	-81.8	-85.5	-82.7	-84.0	-89.9
Ect(HF)	-39.3	-39.0	-38.8	-39.5	-38.6
E2(HF)	-121.1	-124.5	-121,5	-123.5	-128.5

ΔE(B3LYP)	**-632.7**	**-638.5**	**-632.9**	**-635.2**	**-632.8**
ΔE(ωB97X-D)	**-628.4**	**-635.3**	**-628.9**	**-631.5**	**-629.8**
ΔEtot(SIBFA)	**-619.4**	**-631.4**	**-622.2**	**-623.0**	**-631.0**
ΔE(HF)	-592.2	-598.1	-592.3	-594.5	-592.7

Table VII. Dizinc cores of VIM-2 in their complexes with the five inhibitors. ALMOEDA DFT, HF, and SIBFA intermolecular interaction energies and their contributions. Energies in kcal/mol.

	Dizinc core				
	I. Lig-4690	II. Lig-4390	III. Lig-4684	IV. Lig-5064	V. Lig-5069
E1(B3LYP)	**-609.3**	**-619.7**	**-609.3**	**-602.5**	**-625.1**
E1(ωB97X-D)	**-624.4**	**-634.9**	**-624.1**	**-616.9**	**-638.3**
E1(SIBFA)	**-617.6**	**-634.5**	**-622.5**	**-614.9**	**-641.7**
E1(HF)	-607.8	-616.5	-606.6	-598.4	-622.6
Epol(B3LYP)	-262.7	-265.6	-265.7	-273.8	-257.7
Ect(B3LYP)	-129.2	-125.2	-127.3	-129.2	-121.5
E2(B3LYP)	**-391.9**	**-390.8**	**-392.9**	**-403.1**	**-379.2**
Epol(ωB97X-D)	-261.0	-264.3	-264.1	-272.8	-256.2
Ect(ωB97X-D)	-119.6	-117.1	-118.4	-121.1	-113.2
E2(ωB97X-D)	**-380.6**	**-381.4**	**-382.5**	**-393.9**	**-369.4**
Epol(SIBFA)	-271.3	-265.4	-270.6	-270.8	-255.6
Ect(SIBFA)	-60.0	-62.9	-60.7	-64.7	-61.5
E2(SIBFA)	-331.3	-328.3	-331.3	-335.5	-317.0
Edisp(SIBFA)	-35.9	-39.6	-37.1	-41.0	-38.0
E2+Edisp	**-367.2**	**-368.0**	**-368.5**	**-376.5**	**-355.0**
Epol(HF)	-233.8	-236.0	-236.2	-244.0	-228.3
Ect(HF)	-77.8	-77.3	--77.7	-80.7	-74.5
E2(HF)	-311.5	-313.3	-313.9	-324.7	-302.8

ΔE(B3LYP)	**-1001.2**	**-1010.5**	**-1002.2**	**-1005.5**	**-1004.3**
ΔE(ωB97X-D)	**-1004.9**	**-1016.2**	**-1006.6**	**-1010.8**	**-1007.7**
ΔEtot(SIBFA)	**-983.8**	**-1000.8**	**-989.7**	**-989.6**	**-995.2**
ΔE(HF)	-919.4	-929.8	-920.5	-923.1	-925.4

Colored core unbound					
	I. Lig-4690	II. Lig-4390	III. Lig-4684	IV. Lig-5064	V. Lig-5069
E1(B3LYP)	**-471.8**	**-475.5**	**-472.0**	**-472.6**	**-466.3**
E1(ωB97X-D)	**-472.8**	**-476.6**	**-473.2**	**-473.7**	**-467.4**
E1(SIBFA)	**-469.2**	**-478.4**	**-472.2**	**-471.0**	**-473.9**
E1(HF)	-471.1	-473.7	-470.7	-470.9	-464.2
Epol(B3LYP)	-93.6	-97.7	-94.6	-96.0	-102.7
Ect(B3LYP)	-67.3	-65.3	-66.3	-66.6	-63.9
E2(B3 LYP)	**-160.9**	**-163.0**	**-160.9**	**-162.6**	**-166.6**
Epol(ωB97X-D)	-93.1	-97.6	-94.3	-95.8	-102.6
Ect(ωB97X-D)	-62.5	-61.2	-61.4	-62.0	-59.8
E2(ωB97X-D)	**-155.6**	**-158.7**	**-155.7**	**-157.8**	**-162.4**
Epol(SIBFA)	-104.2	-105.5	-105.2	-102.3	-102.6
Ect(SIBFA)	-32.2	-33.0	-31.6	-33.0	-33.2
E2(SIBFA)	-136.4	-136.7	-136.8	-138.0	-140.0
Edisp(SIBFA)	-14.0	-14.9	-13.4	-14.3	-16.0
E2+Edisp	**-150.4**	**-151.5**	**-150.2**	**-152.3**	**-156.0**
Epol(HF)	-81.8	-85.5	-82.7	-84.0	-89.9
Ect(HF)	-39.3	-39.0	-38.8	-39.5	-38.6
E2(HF)	-121.1	-124.5	-121,5	-123.5	-128.5
ΔE(B3LYP)	**-632.7**	**-638.5**	**-632.9**	**-635.2**	**-632.8**

ΔE(ωB97X-D)	**-628.4**	**-635.3**	**-628.9**	**-631.5**	**-629.8**
ΔEtot(SIBFA)	**-619.4**	**-631.4**	**-622.2**	**-623.0**	**-631.0**
ΔE(HF)	-592.2	-598.1	-592.3	-594.5	-592.7

Supp-Info-SI. LSQF-optimized parameters on the triazole-thione fragment.

The atoms of TZT are defined in the following succession:

C2: C atom bearing the R1 substituent;
N3: unsubstituted N atom ortho to it;
N4: unsubstituted N atom meta to C2, which binds to Zn(II) in the Zn1 ('blue') site;
C5: C atom bearing the extracyclic S atom;
N6: N atom ortho to C2 and substituted by the hydrazone group;
S7: extracyclic S atom, which binds to Zn(II) in the Zn2 ('colored') site.

The hydrazone atoms are defined with first the nitrogen, N2, then the carbon, C3.
The first atom on each fragment is always an H atom, denoted as H1.

1. Values of the effective radii for EMTP*, Erep, Epol, Ect, and Edisp.

	EMTP*	Erep	Epol	Ect	Edisp
C2	1.605	1.785	1.700	1.758	1.785
N3	1.536	1.700	1.827	1.850	1.800
N4	1.536	1.700	1.827	1.850	1.800
C5	1.605	1.785	1.700	1.758	1.785
N6	1.601	1.802	1.844	1.580	1.729
S7	1.678	1.340	3.117	2.535	1.340
N2	1.800	1.700	1.529	2.080	1.720
C3	1.499	1.786	1.700	1.758	1.786

2. Internal coordinates of the lone pairs of the triazole-thione and hydrazone fragments.

'popul' denotes the electronic population of the lone pair, incra and incrb denote the increment of the effective radii of the lone pair bearer along the lone pair direction for the short-range repulsion and for the charge-transfer, respectively.

fragment TZT

	theta	phi	R	popul	incra	incrb
C2	124.957	91.340	0.385	0.438	-1.114	0.081
C2	124.957	-88.659	0.385	0.438	-1.114	0.081
N3	140.776	0.039	1.064	1.501	-0.287	-1.209
N3	94.395	48.015	1.146	0.174	-1.526	-0.084
N3	94.395	-47.984	1.146	0.174	-1.526	-0.084

N3	85.856	133.385	-0.167	0.612	1.189	0.789
N3	85.856	226.385	-0.167	0.612	1.189	0.789
N4	107.901	180.172	1.548	1.490	-0.838	-1.002
N4	120.353	227.916	0.887	0.863	0.040	-0.585
N4	120.353	131.916	0.887	0.863	0.040	-0.585
N4	73.595	46.407	-0.410	0.660	-0.101	-0.089
N4	73.595	-46.772	-0.410	0.660	-0.101	-0.089
C5	83.855	108.924	0.665	0.435	0.289	-0.134
C5	83.855	250.924	0.665	0.435	0.289	-0.134
N6	28.157	-89.979	-0.035	0.935	-0.312	0.066
N6	28.157	90.020	-0.035	0.935	-0.312	0.066
S7	108.386	180.041	0.931	0.800	0.939	-0.159
S7	108.386	120.041	0.931	0.800	0.939	-0.159
S7	108.386	60.041	0.931	0.800	0.939	-0.159
S7	108.386	0.041	0.931	0.800	0.939	-0.159
S7	108.386	-59.958	0.931	0.800	0.939	-0.159
S7	108.386	240.041	0.931	0.800	0.939	-0.159

fragment HN=CH2
5

	theta	phi	R	popul	incra	incrb
N2	127.540	180.000	0.727	2.000	-0.200	0.200
N2	45.000	90.000	0.750	0.500	0.350	0.200
N2	45.000	-90.000	0.750	0.500	0.350	0.200
C3	90.000	90.000	0.750	0.500	0.500	-0.225
C3	90.000	-90.000	0.750	0.500	0.500	-0.225

3. Lone-pair and bond polarizabilities.
Ea, Eb, Ec, and Ed denote the multiplicative factors used in the Gaussian screening of the field, for, respectively the bond and the lone pair polarizabilities prior to iterating with the induced dipoles, and for the bond and lone pair polarizabilities upon iterating.

Fa, Fb, Fc, and Fd denote the corresponding Gaussian exponents.

TZT:

Ea	Eb	Ec	Ed	Fa	Fb	Fc	Fd
0.851	0.871	0.885	1.279	2.039	1.057	1.623	3.332

hydrazone:

Ea	Eb	Ec	Ed	Fa	Fb	Fc	Fd
0.851	1.129	0.818	0.705	2.039	1.620	2.048	2.311

Values of the polarizabilities in Angstrom ** 3

TZT. There is one lone-pair polarizability on atoms N3, N4, and N6, and three ones on atom S7. The numbering of the bond polarizabilities is as follows:

9: H1-C2
10: C2-N3
11: C2-N3
12: C2-N6
13: N3-N4
14: N4-C5
15: N4-C5
16: N5-N6
17: N5-N6
18: C5-S7
19: N6-H8

Values of the lone-pair polarizabilities

3	3.813
4	4.101
6	1.658
7	11.836
7	4.862
7	6.872

Values of the bond polarizabilities

9	0.000
10	11.132
11	6.579
12	2.179
13	2.629
14	3.229
15	3.161
16	1.849
17	1.915
18	1.593
19	2.141

Hydrazone. There is one lone-pair polarizability on atom N2.
The numbering of the bond polarizabilities is as follows:

6: H1-N2
7: N2-C3
8: C3-H4
9: C3-H5

Value of the lone-pair polarizability
2 12.804

Value of the bond polarizabilities
6 0.000
7 2.534
8 0.727
9 3.450

Supp. Info S2. Distances (in Angstrom units) between Zn(II) and its ligands in the dizinc core. Values in parentheses in the Lig-4690 column correspond to the ones determined by X-ray crystallography.

	I. Lig-4690	II. Lig-4390	III. Lig-4684	IV. Lig-5064	V. Lig-5069
Zn1-H116	2.01 (2.02)	1.92	1.99	1.87	2.02
Zn1-H118	2.16 (1.90)	2.13	1.96	2.12	2.18
Zn1-H196	1.97 (2.08)	1.94	2.03	1.88	1.94
Zn1-N(TZT)	1.92 (1.91)	1.93	2.28	1.88	1.98
Zn2-D120	1.97 (2.08)	1.99	1.93	1.96	2.08
Zn2-C221	2.30 (2.16)	2.23	2.32	2.27	2.33
Zn2--H263	2.48 (2.31)	2.30	2.48	2.46	2.00
Zn2-S(TZT)	2.06 (2.25)	2.07	2.07	2.08	2.35

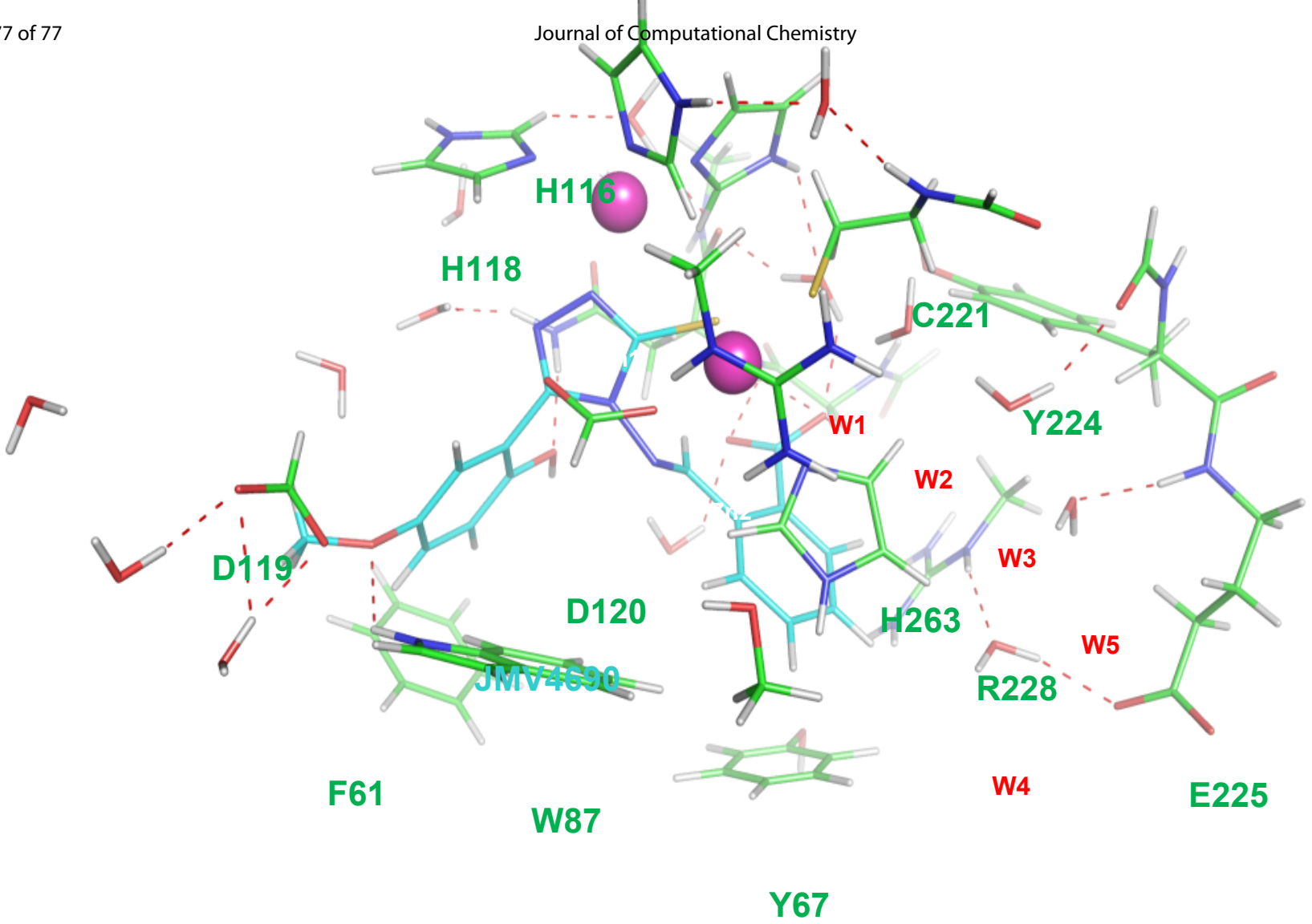

VIM-2 is a bacterial Zn-metallo-beta-lactamase, responsible for nosocomial infections. We consider its complexes with five novel inhibitors sharing a triazole-thione anchoring group. For each of these, we validate a polarizable molecular mechanics/dynamics potential against ab initio QC computations. The test cases embody the interactions in the two mono-zinc sites and in the di-zinc site, up to the entirety of the extended recognition site, which totals up to 280 atoms.